natriuretic peptides are potential therapeutic targets for heart disease (9–14).

Mice transgenic for various loci, including the 5′-flanking regions of the natriuretic peptide genes, have been used to identify the regulatory elements required for transcriptional activation either during heart development or in the diseased heart. These studies reported that the 5′-flanking regions of the natriuretic peptide genes regulated their expression during heart development (9, 10, 13); however, the 5′-flanking regions were not responsible for their specific reactivation in the diseased heart (11, 12). A recent study identified the distal enhancer elements regulating the natriuretic peptide genes in the developing heart by examining cardiac-specific transcription factor binding sites; however, these enhancer elements did not respond to heart failure (14). Therefore, the stress-responsive regulatory elements that function during heart failure have not yet been identified and are potentially located outside the 5′-flanking regions.

In this study, we aimed to identify the novel stress-responsive enhancer elements of the *Nppa* and *Nppb* genes in the failing heart. Furthermore, we established a noninvasive and quantitative live imaging assay to monitor the transcriptional activity of candidate enhancers in the failing heart. *In vivo* live imaging of the firefly luciferase reporter in a single mouse enabled us to analyze the sequential changes in enhancer activity during the progression of heart failure. Combined with a fine mapping technique using epigenetic markers, we identified a 650-bp stress-responsive enhancer that was strongly activated by cardiac hypertrophy and heart failure.

MATERIALS AND METHODS

Animals

All procedures were performed according to the U.S. National Institutes of Health (NIH) Guide for the Care and Use of Laboratory Animals (NIH publication no. 85-23, revised 1996) and were approved by the Animal Experiments Committee, Osaka University (approval no. 21-78-10).

Reagents and antibodies

Phenylephrine (PE) was purchased from Sigma-Aldrich (St. Louis, MO, USA). The anti-RNA polymerase II and anti-histone H3 trimethylated at lysine 4 (H3K4me3) antibodies used for chromatin immunoprecipitation sequencing (ChIP-seq) were kind gifts from Dr. H. Kimura (Graduate School of Frontier Biosciences, Osaka University).

Primary culture of neonatal rat cardiomyocytes

Ventricular myocytes obtained from 1- or 2-d-old Wistar rats were prepared and cultured overnight in Dulbecco's modified Eagle's medium (Sigma-Aldrich) containing 10% FBS, as described previously (15).

Comparative genomics

Genome-wide multiple alignments of the genomic sequences containing the *Nppa* and *Nppb* genes were performed using the University of California Santa Cruz (UCSC) Genome Browser (16); 8 vertebrate species were compared, including mouse (mm9, July 2007), rat (m4, Nov. 2004), human (hg18, Mar. 2006), orangutan (ponAbe2, July 2007), dog (canFam2, May 2005), horse (equCab1, Jan. 2007), opossum (monDom4, Jan. 2006), and chicken (galGal3, May 2006). We used vertebrate Multiz alignment of DNA sequences (17) to analyze the homology of DNA sequences among mouse and other species. We used the Placental Mammal Basewise Conservation assessed by PhyloP (18) to assess the degree of mammalian conservation. Next, we identified discrete conserved fragments. The transcribed sequences within the conserved set were filtered out using known genes, spliced ESTs, and mRNA annotations obtained from the UCSC genome browser. Finally, we manually curated the data set to remove any additional false positives by visual examination of the UCSC genomic data. We defined the noncoding conserved regions (CRs) that were homologous at least in the human and mouse genomes and at least 1 kb away from the transcription start sites as the enhancer candidates.

ChIP sequencing on mouse heart tissues

Whole hearts were isolated from 8-wk-old C57BL6 mice, perfused rapidly with cold PBS, flash-frozen in liquid nitrogen, homogenized using a sterile tissue grinder, and cross-linked with 0.3% paraformaldehyde. Subsequently, chromatin isolation, sonication, and immunoprecipitation using an anti-RNA polymerase II antibody and an anti-H3K4me3 antibody were performed. The ChIP DNA and input samples were sheared by sonication, end-repaired, ligated to the sequencing adapters, and amplified. The purified ChIP DNA library samples were sequenced using the Illumina Genome Analyzer II (Illumina, Inc., San Diego, CA, USA). Unfiltered sequence reads were aligned to the mouse reference genome [U.S. National Center for Biotechnology Information (NCBI) build 37, mm9] using Bowtie. RNA polymerase II- and H3K4me3-enriched regions were identified using MACS (19) with the default parameters.

Lentiviral enhancer assay

Eleven CRs were PCR amplified from the mouse BAC clone containing the *Nppa* and *Nppb* loci (clone RP23-128E8; BACPAC Resources Center, Children's Hospital Oakland, Oakland, CA, USA; primers and probes are listed in Supplemental Table S1). The PCR fragments were subcloned into the pCR-Blunt II-TOPO vector (Invitrogen, Carlsbad, CA, USA) and recombined into a lentiviral vector encoding the firefly luciferase reporter (pGreenFire Transcriptional Reporter Lentivector; System Biosciences, Mountain View, CA, USA). The lentiviral particles were produced by transfection of 293T cells with the 3 lentiviral packaging plasmids (*i.e.*, pMDLg/pRRE, pRSV-Rev, and pMD2.VSV.G) using Lipofectamine 2000 (Invitrogen). The supernatant from 293T cells containing the lentiviral particles was collected 48 h after transfection, sterilized using a 0.45-μm cellulose acetate filter, and concentrated by centrifugation (Peg-it Virus Precipitation Solution, System Biosciences).

Rat neonatal cardiomyocytes isolated as described above were plated in 96-well plates. The next day, the medium was replaced with a serum-free medium containing the lentiviral vector, and the cells were incubated for 12 h. Subsequently, the cardiomyocytes were exposed to 100 μM PE for 48 h prior to the luciferase assay.

RNA extraction and quantitative RT-PCR

The total RNA was prepared from rat cardiomyocytes, rat cardiac fibroblasts, murine hearts, and murine brains using the RNA-Bee RNA isolation reagent (Tel-Test, Friendswood, TX, USA) and then converted to cDNA using the high-capacity cDNA reverse transcription kit (Applied Biosystems, Foster City, CA, USA), according to the manufacturer's instructions. The quantitative RT-PCR was performed using the TaqMan technology and the StepOnePlus real-time PCR System (Applied Biosystems). All samples were processed in duplicate. The level of each transcript was quantified according to the threshold cycle (C_t) method using GAPDH as an internal control. Inventoried TaqMan gene expression assays were used: *Nppa*, Rn0056661, Mm01255748; *Nppb*, Rn00580641, Mm01255770; *Gapdh*, rodent GAPDH control reagent.

3C analysis

The whole hearts of the mice were isolated, perfused rapidly with cold PBS, flash-frozen in liquid nitrogen, homogenized using a sterile tissue grinder, and fixed with 1% paraformaldehyde. The cross-linked tissues utilized for 3C experiments were subjected to digestion with *Bam*HI following standard protocols (20, 21). The mouse BAC DNA containing *Nppa* and *Nppb* (clone RP23-128E8) was used as a control. The TaqMan real-time PCR was performed using probes near the restriction sites; the primers and probes are listed in Supplemental Table S2.

Transgenic mouse enhancer assay

The candidate enhancer regions were cloned into a vector encoding the minimal CMV promoter driving the luciferase gene as described above. Transgenic mouse embryos were generated by pronuclear injection into the zygotes of BDF1 mice using standard methods. Because black fur attenuates light transmission, albino mice were generated by crossing the transgenic founders to ICR albino mice.

In vivo bioluminescence imaging

Prior to *in vivo* imaging, the mice were anesthetized using isoflurane, and the black mice were shaved from the neck to the lower torso to allow the optimal visualization of fluorescence without interference from the black fur. A D-luciferin solution was injected intraperitoneally (150 mg/kg i.p.) or intravenously (75 mg/kg i.v.). The mice were imaged using an *in vivo* live imaging system (IVIS Lumina II; Caliper Life Sciences, Waltham, MA, USA). For quantification, the bioluminescence light intensity was measured at the region of interest and expressed in relative light units (RLU/min) using Living Image 4.0 (Caliper Life Sciences). To calculate the enhancer activity in the heart, we defined the ratio of heart to brain luciferase intensities as the cardiac-specific enhancer activity.

Transverse aortic constriction (TAC)

Transgenic mice aged 8 wk and weighing 20–25 g were subjected to pressure overload, as described previously (22). Briefly, the chest was entered *via* the second intercostal space at the upper left sternal border. After the arch of the aorta was isolated, a TAC was created using a 7-0 suture tied twice around a 27-gauge needle and the aortic arch, between the innominate and left common carotid arteries. After the suture was tied, the needle was gently removed, yielding 60–80% constriction of the aorta.

PE-induced hypertrophy

Transgenic mice aged 8 wk and weighing 20–25 g were treated with PE (75 mg/kg/d) using an osmotic minipump (Alzet, Cupertino, CA, USA) to induce cardiac hypertrophy, as previously reported (23, 24).

Statistical analysis

Data are expressed as means ± SE. The 2-tailed Student's *t* test and repeated ANOVA were used to analyze differences between the groups. Values of $P < 0.05$ were considered to represent a significant difference.

RESULTS

Identification of candidate enhancers near the *Nppa-Nppb* locus using comparative genomics and ChIP-seq

To identify potential enhancers, we performed a comparative analysis of the genomic sequences of mouse and divergent species and identified CRs that may function as common regulatory sequences (25–27). We defined CRs that were homologous at least in the human and mouse genomes and at least 1 kb away from the transcription start sites of *Nppa* and *Nppb* as the candidate enhancers. First, we analyzed the 50-kb *Nppa-Nppb* locus bounded by the binding sites of 2 CCCTC-binding factors (CTCFs), which can function as insulators (28, 29). Using a genome database (30), we identified 11 CRs, including the *Nppa* and *Nppb* introns in the 50-kb region (**Fig. 1**).

Next, we performed a ChIP-seq analysis on RNA polymerase II and H3K4me3 in the adult mouse heart. We analyzed the epigenetic modifications near the *Nppa* and *Nppb* genes combined with the ChIP-seq analysis using a public database of the adult mouse heart (30). We hypothesized that the normal heart would have activated epigenetic marks because *Nppa* and *Nppb* are expressed, albeit at low levels, in normal conditions. Recent genome-wide studies have determined that enhancers can be defined as DNA sequences bound by the RNA polymerase II and transcriptional coactivator protein p300, and where histone H3 monomethylated at lysine 4 (H3K4me1) accumulates instead of H3K4me3 (31–34). Among the 11 CRs identified, only CR9 coincided with the binding sites of RNA polymerase II and p300, and overlapped with the gene areas modified by H3K4me1, and filled all criteria for the enhancer (Fig. 1). In addition, H3K4me1 modifications in CR9 were only observed in the heart but not in the other organs (Fig. 1 and Supplemental Fig. S1). Therefore, we analyzed the 11 CRs, including CR9, as the most likely distal candidate enhancers for the stress-responsive regulatory regions of the natriuretic peptide genes.

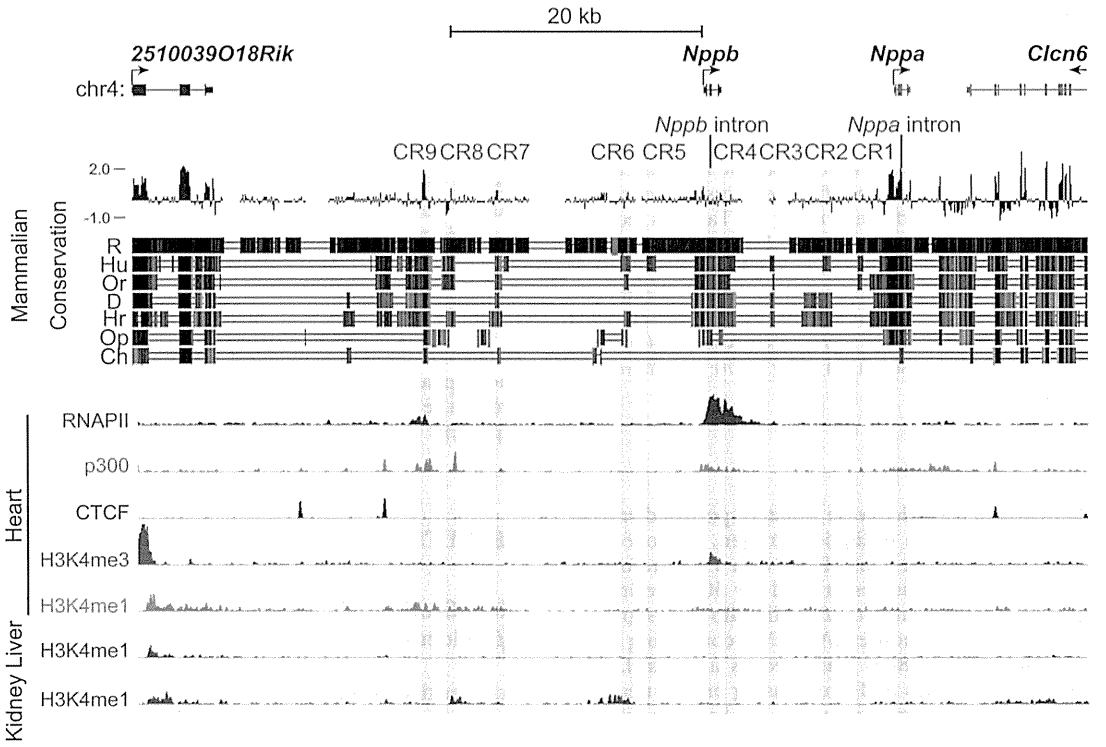

Figure 1. Mammalian evolutionarily conserved regions and ChIP-seq data surrounding the murine *Nppa* and *Nppb* loci. We used an open database on the University of California Santa Cruz (UCSC) Genome Browser to assess the degree of DNA sequence conservation around *Nppa* and *Nppb* gene loci. Blue and red vertical lines, the Placental Mammal Basewise Conservation assessed by PhyloP; black vertical lines, the vertebrate Multiz alignment of DNA sequences among mice and 7 other species (rats, humans, orangutans, dogs, horses, opossums, and chickens). We defined noncoding conserved regions (CRs) that were homologous at least in the human and mouse genomes and at least 1 kb away from the transcription start sites of *Nppa* and *Nppb* as the candidate enhancers. CRs are highlighted as light red vertical bars (CR1-9, *Nppa* intron, and *Nppb* intron). ChIP-seq data for H3K4me1, p300, and CTCF were obtained from an open database of the adult mouse heart. Some CRs coincided with the peaks for H3K4me1, RNA polymerase II, and the transcriptional coactivator protein p300. R, rat; Hu, human; Or, orangutan; D, dog; Hr, horse; Op, opossum; Ch, chicken.

Identification of a distal enhancer element responsive to an α_1-adrenergic receptor agonist

We screened the candidate enhancers for potential stress-responsive regulatory regions. We analyzed the enhancer activity of these 11 CRs after treatment with PE, an α_1-adrenergic receptor agonist, which mimics cardiac overload and induces *Nppa* and *Nppb* expression in cardiomyocytes (35). We confirmed that PE induced the expression of endogenous *Nppa* and *Nppb* specifically in cardiomyocytes but not in cardiac fibroblasts (**Fig. 2*A***). Then, we introduced the 11 CRs with a minimum human cytomegalovirus (CMV) promoter and the luciferase gene into rat cardiomyocytes using a lentiviral vector system.

Among the 11 CRs tested, only CR9, which is located 22 kb upstream from the *Nppb* transcription start site and shows high mammalian conservation score in the Placental Mammal Basewise Conservation by PhyloP (Fig. 2*B*), reproducibly increased the PE-induced luciferase activity by ~5-fold compared to the minimal CMV promoter alone (Fig. 2*C*). However, CR9 did not respond to PE in cardiac fibroblasts (Fig. 2*C*). These results suggest that CR9 is the regulatory element that is responsive to PE specifically in cardiomyocytes.

Long-range physical interaction between the distal enhancer element and the proximal promoters of the *Nppa* and *Nppb* genes

Confirming the looping interactions between distal elements and promoters is one way to demonstrate the transcriptional regulatory activity of distal elements. We performed a 3C assay (20) to comprehensively investigate whether the genomic region containing CR9 moved closer to the *Nppa* or *Nppb* promoter in an adult murine heart treated with a continuous infusion of PE *in vivo*.

The ligation frequencies were quantified by TaqMan real-time PCR using specific primers and probes and were compared to the ligation frequency of noncross-linked *Bam*HI-digested BAC DNA containing the *Nppa-Nppb* locus. We observed that CR9 interacts with both the *Nppa* and *Nppb* promoter regions at a higher frequency relative to other gene areas (Fig. 2*D*); furthermore, PE treatment strengthened these interac-

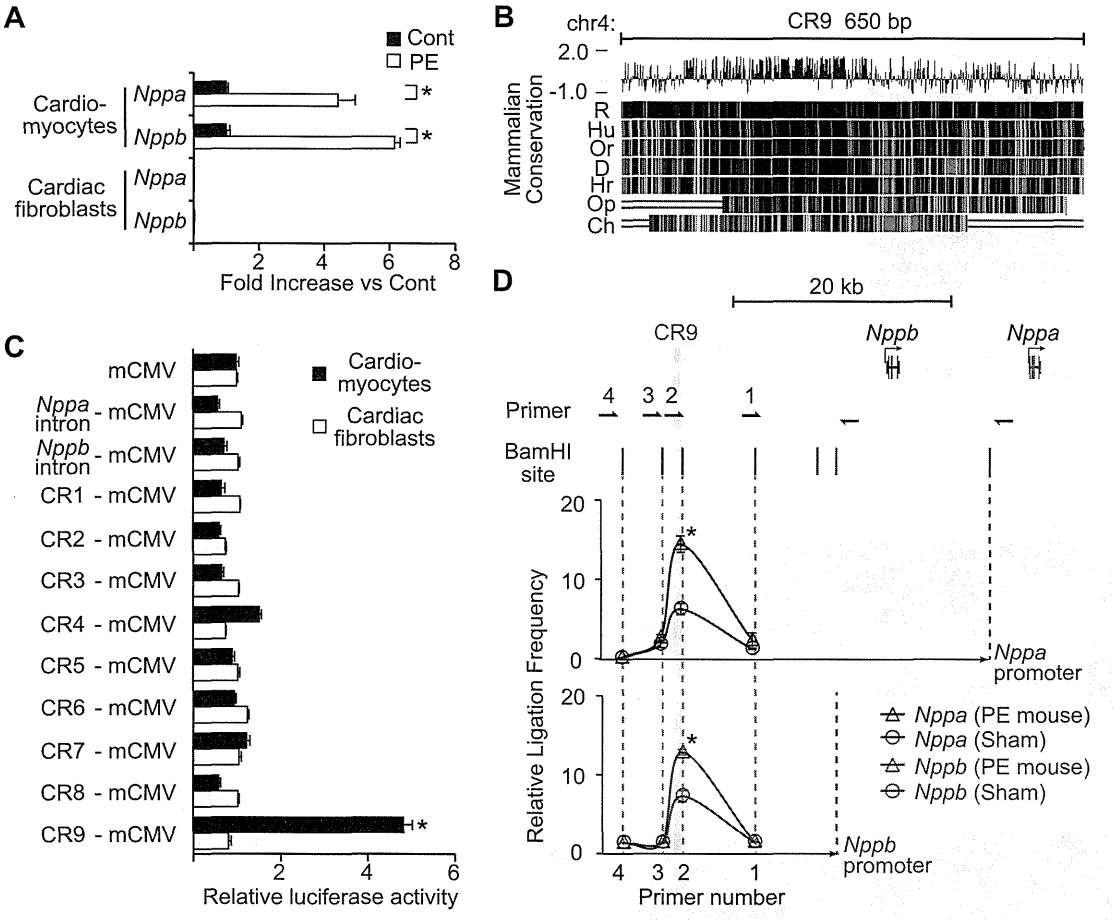

Figure 2. Identification of a distal enhancer element that is responsive to an α_1-adrenergic receptor agonist. *A*) Relative transcript levels of *Nppa* and *Nppb* in rat neonatal cardiomyocytes and cardiac fibroblasts 48 h after treatment with PE (100 μM). Values are means ± SE (n=3 cultures). *$P < 0.01$ *vs.* control; *t* test. *B*) CR9 is a highly conserved genomic region in vertebrates. *C*) Relative luciferase reporter activities of CRs in rat neonatal cardiomyocytes and cardiac fibroblasts 48 h after treatment with PE (100 μM). PE-induced luciferase activity driven by the mCMV promoter was defined as 1. Values are means ± SE (n=5 cultures). *$P < 0.001$ *vs.* mCMV alone; *t* test. *D*) *In vivo* 3C analysis of the murine *Nppa* and *Nppb* loci, showing relative ligation frequencies of each primer to the *Nppa* promoter (blue triangle, mouse with PE treatment; blue circle, mouse without PE) and the *Nppb* promoter (red triangle, mouse with PE treatment; red circle, mouse without PE). Vertical bars and arrows show the positions of *Bam*HI sites and primers. Data were normalized to the amplification value of a *Bam*HI-digested and religated BAC clone, which included the *Nppa* and *Nppb* loci (means ± SE; n=2 hearts). R, rat; Hu, human; Or, orangutan; D, dog; Hr, horse; Op, opossum; Ch, chicken. *$P < 0.05$ *vs.* control; *t* test.

tions (Fig. 2*D*). These results suggest that there is a close proximity between the distal genomic region containing CR9 and the proximal promoters of the *Nppa* and *Nppb* genes in the PE-induced hypertrophic heart.

Establishment of an *in vivo* live imaging system for gene expression in a murine model of heart disease

We confirmed the activity of the newly identified enhancer CR9 in the heart *in vivo*. The conventional histological evaluation of LacZ reporter expression in the heart only provides data at a single time point; therefore, this method cannot be employed for kinetic assessments or time course analyses of reporter expression in a live heart.

To overcome this difficulty, we established a noninvasive and quantitative live imaging system that allowed real-time monitoring of the firefly luciferase reporter. We generated 3 transgenic mouse lines (Tg-line1, Tg-line2, and Tg-line3) in which the CR9 enhancer element and a minimal CMV promoter driving the luciferase reporter gene were introduced into the germline. The live-imaging system detected luciferase expression in the heart, brain, and intestine of the Tg-line1 (**Fig. 3*A***), in the heart, salivary glands, and skin of the Tg-line2 (Supplemental Fig. S2*A*), and in the heart of the Tg-line3 (Supplemental Fig. S2*E*).

To identify the organs in which CR9 functioned as a stress-responsive enhancer, we examined the luciferase reporter expression in each organ by quantitative PCR. Continuous infusion of PE increased the blood pressure and resulted in cardiac hypertrophy (24, 36). The

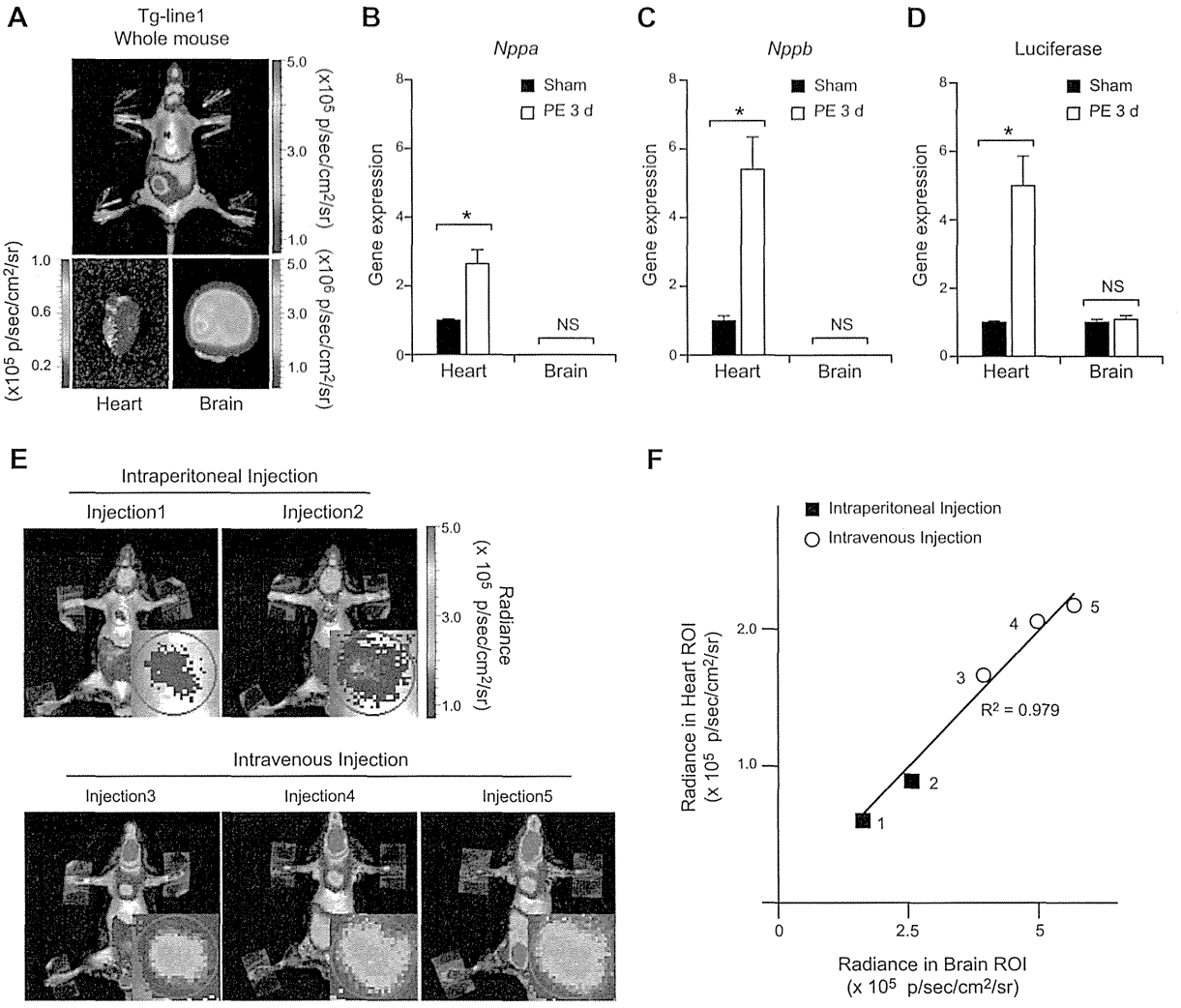

Figure 3. Establishment of an *in vivo* live imaging system for enhancer activity. *A*) Chemiluminescence imaging of CR9 in a mouse of Tg-line1. Top panel: result from whole-animal *in vivo* live imaging. Bottom panels: chemiluminescence images of the heart and brain in the same mouse. *B, C*) Relative transcript levels of *Nppa* and *Nppb* in the ventricular myocardium and brain of CR9 Tg-line1 mice treated with continuous infusion of PE for 3 d. Average transcript level in the ventricular myocardium of preinfused mice was defined as 1 (means ± SE; n=5 hearts). *$P < 0.01$ *vs.* sham-infused mice; *t* test. *D*) Relative transcript levels of luciferase reporter in the ventricular myocardium and brain of the CR9 Tg-line1 mice continuously infused with PE for 3 d. Average transcript level in the ventricular myocardium and brain of preinfused mice was defined as 1. (means ± SE; n=5 hearts). *$P < 0.01$ *vs.* sham-infused mice; *t* test. *E*) Comparison of the chemiluminescence intensities obtained using different luciferin injection methods in a Tg-line1 mouse; injections 1 and 2, intraperitoneal injections (top panels), injections 3, 4, and 5, intravenous injections (bottom panels). Injections were performed ≥4 h apart to eliminate the effect of the previous injection. Inset in each panel shows a magnified image of the heart. *F*) Scatterplots of the chemiluminescence intensities in the heart and brain. Plots indicate the independent experiments shown in each panel in *E*. There is a linear relationship between the expression in the heart and the brain, $R^2 = 0.979$.

expression of endogenous *Nppa* and *Nppb* mRNA increased 3 d after the PE infusion began (Fig. 3*B, C* and Supplemental Fig. S2*B, C, F, G*). Concomitantly, the quantitative PCR analysis of the CR9 luciferase mRNA expression showed enhanced expression in the ventricular myocardium 3 d after the PE infusion (Fig. 3*D* and Supplemental Fig. S2*D, H*). On the other hand, in the brain and the salivary glands where neither *Nppa* nor *Nppb* is highly expressed, the CR9-driven luciferase mRNA expression did not respond to PE (Fig. 3*B–D* and Supplemental Fig. S2*B–D, F–H*). Therefore, the patterns of PE-induced luciferase expression suggest that CR9 is almost exclusively active in the heart. Because the integration sites were random in these three lines, the patterns of luciferase expression depend on CR9 or other enhancers near the integrated sites. The expression of luciferase in the brain of Tg-line1 and salivary glands of Tg-line2, both of which express neither *Nppa* nor *Nppb,* might be driven by other enhancers near the integrated sites.

To evaluate the accuracy and reproducibility of this method, we measured the luminescence in the heart of

a mouse from Tg-line1. In this transgenic line, the brain, intestine, and testis expressed the reporter protein due to positional effects of the insertion site and most likely not due to CR9 activity. Because the luciferase mRNA expression in the brain remained unchanged after PE treatment (Fig. 3*D*), we used the reporter activity in the brain as a control. The absolute luminescence values of the heart were affected by the injection method and the amount of luciferase substrate injected (Fig. 3*E*). However, using brain luminescence as a control, we successfully eliminated the signal variations caused by these differences. The ratio of the luminescence in the heart and brain remained constant within each mouse, independent of the injection method (Fig. 3*F*). Therefore, we defined the ratio of heart to brain luciferase intensities as the cardiac-specific enhancer activity.

Distal enhancer element was activated in the murine model of heart failure

To examine whether the CR9 enhancer was also responsible for gene expression in other pathological conditions, we subjected Tg-line1 mice to heart failure induced by TAC and compared them with sham-surgery mice. This model mimics the heart condition of patients with hypertension who suffer a continuous pressure overload on the heart. The pressure overload by TAC caused potent cardiac hypertrophy at 2 wk postsurgery and reduced cardiac contractility at 3 wk postsurgery (**Fig. 4*A*, *B***), as previously reported (22). The endogenous *Nppa* and *Nppb* expression increased severalfold in the ventricular myocardium 3 wk after the TAC surgery (Fig. 4*C*). The heart to brain luciferase intensity ratio also increased severalfold 3 wk following the TAC surgery (Fig. 4*D*, *E* and Supplemental Fig. S3). However, the heart to brain luciferase intensity ratio of sham-surgery mice did not change after the surgery (Fig. 4*D*, *E* and Supplemental Fig. S3; 3 wk after TAC surgery: 5.7±1.3 fold; 3 wk after sham surgery: 1.0±0.2 fold; $P < 0.001$, repeated ANOVA). These results suggest that CR9 increases transcriptional activity during mechanical pressure overload-induced hypertrophy and subsequent heart failure.

DISCUSSION

Here, we focused on the stress-responsive regulatory elements of *Nppa* and *Nppb* in heart failure. By screening the evolutionarily conserved and epigenetically modified regions around the *Nppa* and *Nppb* gene loci, we identified a 650-bp transcriptional enhancer that was responsive to an α_1-adrenergic receptor agonist *in vitro*. Furthermore, *in vivo* 3C analysis revealed that this distal enhancer directly interacted with the 5′-flanking regions of both *Nppa* and *Nppb*. Using *in vivo* live imaging of luciferase reporter gene expression, we observed that this 650-bp enhancer caused cardiac-specific activation of reporter gene expression during the progression of pressure overload-induced heart failure. Notably, this is the first study to provide a time series analysis for monitoring enhancer activity under pathological conditions in an individual live mouse.

Although numerous approaches have been used to explore the stress-responsive regulatory elements driving gene transcription during heart failure (11, 12, 14), these elements have not yet been identified due to the technical difficulty involved. To detect the elements that are responsive to pathological conditions such as heart failure, it is essential to confirm the activity of the responsive element using a beating heart that remains connected to the systemic cardiovascular system. Therefore, it would be beneficial to establish transgenic mouse lines carrying a reporter plasmid to assess the responsive elements driving the expression of specific genes. However, the creation of multiple stable adult mouse lines to identify these elements is time-consuming.

In this study, we utilized two improved methods for reporter analysis and successfully identified a novel potent enhancer.

First, by performing an enhancer analysis using a lentiviral vector, we accurately identified candidate enhancers in cardiomyocytes and subsequently generated transgenic reporter mice. Previous promoter analyses used electroporation or lipofection to transfect cultured cardiomyocytes with plasmids (37, 38), but the transfection efficiency of these methods in primary cardiomyocytes is too low to accurately measure reporter activity during the stress response. In this study, greater than 90% transduction efficiency of cardiomyocytes was achieved using a lentiviral vector, which enabled us to accurately identify a specific enhancer fragment. Using this method, we efficiently minimized the number of reporter plasmids to be subsequently integrated into the mouse genome to screen for potential enhancers.

Second, by sequentially measuring the enhancer activity in a single live mouse, we collected robust data to assess enhancer activity in the heart *in vivo*. LacZ is not a suitable reporter for this purpose because LacZ activity can only be assessed after animal euthanization. Therefore, we overcame this limitation using the luciferase reporter plasmid. Recent advances in high-sensitivity luminescence imaging have made it possible to evaluate enhancer-driven luciferase activity without operating on the mice. Therefore, we sequentially assessed reporter activity and hemodynamic changes in the same mouse throughout the time course of the development of heart failure. These data were highly reproducible and enabled us to identify an enhancer element that was activated by cardiac overload. Because this method can be applied to any organ, the *in vivo* luciferase reporter assay may be used for assessing the *in vivo* enhancer or promoter activities responsible for clinically important diseases. The noninvasive nature of this method also enabled us to simultaneously assess the hemodynamic and metabolic parameters *in vivo* along with reporter activity. Specifically, the Tg-line1

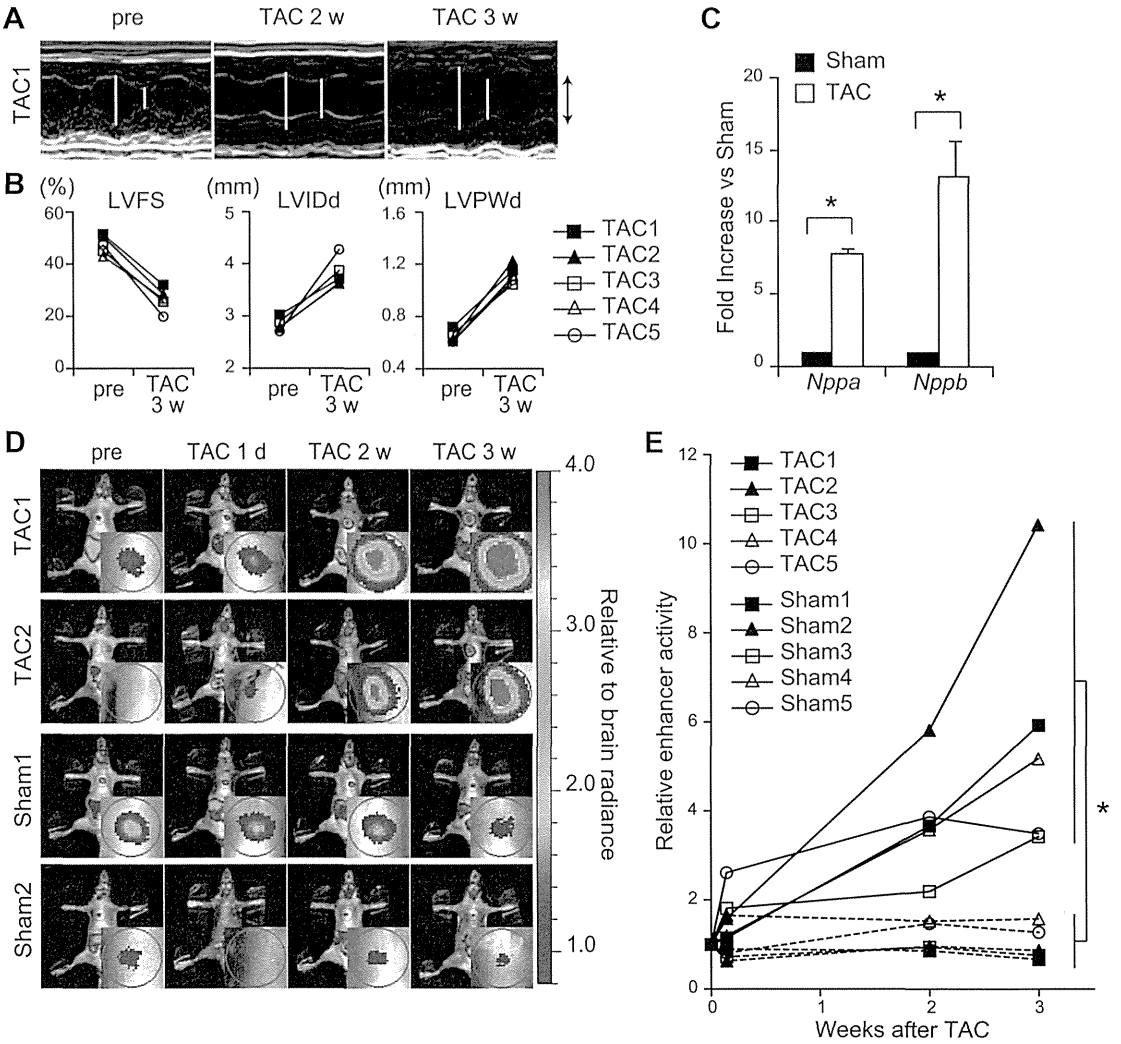

Figure 4. Distal enhancer element is reactivated in the murine model of heart failure. *A*) Representative M-mode echocardiograms in a mouse of Tg-line1 (TAC1) before and after TAC. Open bars indicate maximal left ventricular internal dimension in diastole (LVIDd) and maximal left ventricular internal dimension in systole (LVIDs). Up and down arrows represent 3 mm. *B)* Echocardiographic changes in left ventricular fractional shortening (LVFS), LVIDd, and left ventricular posterior wall thickness in diastole (LVPWd) in 5 mice of Tg-line1 (TAC1-5) before and after TAC. *C*) Relative *Nppa* and *Nppb* transcript levels in the ventricular myocardium 3 wk after the TAC procedure (means ± SE; n=3 hearts). *$P < 0.05$ *vs.* sham-surgery mice; *t* test. *D*) Sequential *in vivo* live imaging of 4 representative Tg-line1 mice before and after TAC or sham surgery at each time point. Top 2 and bottom 2 panels represent sequential imaging data of TAC and sham-surgery mice, respectively. Sequential imaging of the 6 other surgically treated mice is shown in Supplemental Fig. S3. Insets in images show magnified images of the heart. Color scale depends on the ratio relative to brain intensity. *E*) Cardiac-specific enhancer activity plots of 10 Tg-line1 mice (TAC1, TAC2, and Sham1, Sham2, shown in *D*) and TAC3–5 and Sham3–5 shown in Supplemental Fig. S3). Heart to brain luciferase intensity ratio represents the cardiac-specific enhancer activity; enhancer activity in presurgery mice was defined as 1. 3 wk after TAC surgery: 5.7 ± 1.3 fold; 3 wk after sham surgery: 1.0 ± 0.2 fold; means ± SE; n = 5. *$P < 0.001$, repeated ANOVA.

mice enabled us to accurately quantify the expression level of the natriuretic peptides. These mice are useful tools for repeatedly assessing the degree of heart failure to screen various cardiovascular drugs.

The integration of activities from multiple enhancers could confer specificity and robustness to transcriptional regulation (1). Warren *et al.* (14) identified the *Nppa* enhancer in the embryonic heart by examining Nkx2-5 binding regions around the *Nppa* locus, but the enhancer did not respond to heart failure. This enhancer does not overlap with CR9 and might regulate *Nppa* expression only during the embryonic stage (14). On the other hand, Horsthuis *et al.* (11) showed that the regulatory region from −27 to +58 kb relative to the transcription start site of *Nppa* was sufficient for *Nppa* gene expression in the failing heart, similar to CR9. However, because this 85-kb regulatory region does not include CR9, *Nppa* may have multiple enhanc-

ers that regulate its expression during heart failure. Furthermore, the length of the 85-kb region poses a challenge for understanding its specific biological role.

This is the first study to provide a time course imaging analysis of enhancer activity using an individual live diseased mouse model. Using this new method, we identified a novel heart enhancer. This method can be widely used for identifying enhancers that regulate transcriptional activity only under pathological conditions. FJ

This research was supported by the Japan Society for the Promotion of Science (JSPS) through the Funding Program for Next Generation World-Leading Researchers (NEXT Program), which was initiated by the Council for Science and Technology Policy (CSTP); grants-in-aid from the Ministry of Health, Labor, and Welfare of Japan; grants-in-aid from the Ministry of Education, Culture, Sports, Science, and Technology of Japan; and grants-in-aid from the Japan Society for the Promotion of Science. This research was also supported by grants from the Japan Heart Foundation, the Japan Cardiovascular Research Foundation, the Japan Medical Association, the Japan Intractable Diseases Research Foundation, the Uehara Memorial Foundation, the Takeda Science Foundation, the Ichiro Kanehara Foundation, the Inoue Foundation for Science, the Mochida Memorial Foundation, a Heart Foundation/Novartis Grant for Research Award on Molecular and Cellular Cardiology, the Japan Foundation of Applied Enzymology, the Naito Foundation, the Banyu Foundation, and Showa Houkoukai. The authors thank Hiroshi Kimura for antibodies, Seitaro Nomura for the ChIP-seq analysis, Saori Ikezawa and Eri Takata for technical assistance, and Yuko Okada and Hiromi Fujii for secretarial support.

REFERENCES

1. Spitz, F., and Furlong, E. E. (2012) Transcription factors: from enhancer binding to developmental control. *Nat. Rev. Genet.* **13,** 613–626
2. Chien, K. R., Domian, I. J., and Parker, K. K. (2008) Cardiogenesis and the complex biology of regenerative cardiovascular medicine. *Science* **322,** 1494–1497
3. Olson, E. N. (2006) Gene regulatory networks in the evolution and development of the heart. *Science* **313,** 1922–1927
4. Burley, D. S., and Baxter, G. F. (2007) B-type natriuretic peptide at early reperfusion limits infarct size in the rat isolated heart. *Basic Res. Cardiol.* **102,** 529–541
5. Holtwick, R., van Eickels, M., Skryabin, B. V., Baba, H. A., Bubikat, A., Begrow, F., Schneider, M. D., Garbers, D. L., and Kuhn, M. (2003) Pressure-independent cardiac hypertrophy in mice with cardiomyocyte-restricted inactivation of the atrial natriuretic peptide receptor guanylyl cyclase-A. *J. Clin. Invest.* **111,** 1399–1407
6. Kitakaze, M., Asakura, M., Kim, J., Shintani, Y., Asanuma, H., Hamasaki, T., Seguchi, O., Myoishi, M., Minamino, T., Ohara, T., Nagai, Y., Nanto, S., Watanabe, K., Fukuzawa, S., Hirayama, A., Nakamura, N., Kimura, K., Fujii, K., Ishihara, M., Saito, Y., Tomoike, H., and Kitamura, S. (2007) Human atrial natriuretic peptide and nicorandil as adjuncts to reperfusion treatment for acute myocardial infarction (J-WIND): two randomised trials. *Lancet* **370,** 1483–1493
7. Li, P., Wang, D., Lucas, J., Oparil, S., Xing, D., Cao, X., Novak, L., Renfrow, M. B., and Chen, Y. F. (2008) Atrial natriuretic peptide inhibits transforming growth factor beta-induced Smad signaling and myofibroblast transformation in mouse cardiac fibroblasts. *Circ. Res.* **102,** 185–192
8. Tamura, N., Ogawa, Y., Chusho, H., Nakamura, K., Nakao, K., Suda, M., Kasahara, M., Hashimoto, R., Katsuura, G., Mukoyama, M., Itoh, H., Saito, Y., Tanaka, I., Otani, H., and Katsuki, M. (2000) Cardiac fibrosis in mice lacking brain natriuretic peptide. *Proc. Natl. Acad. Sci. U. S. A.* **97,** 4239–4244
9. De Lange, F. J., Moorman, A. F., and Christoffels, V. M. (2003) Atrial cardiomyocyte-specific expression of Cre recombinase driven by an Nppa gene fragment. *Genesis* **37,** 1–4
10. Habets, P. E., Moorman, A. F., Clout, D. E., van Roon, M. A., Lingbeek, M., van Lohuizen, M., Campione, M., and Christoffels, V. M. (2002) Cooperative action of Tbx2 and Nkx2.5 inhibits ANF expression in the atrioventricular canal: implications for cardiac chamber formation. *Genes Dev.* **16,** 1234–1246
11. Horsthuis, T., Houweling, A. C., Habets, P. E., de Lange, F. J., el Azzouzi, H., Clout, D. E., Moorman, A. F., and Christoffels, V. M. (2008) Distinct regulation of developmental and heart disease-induced atrial natriuretic factor expression by two separate distal sequences. *Circ. Res.* **102,** 849–859
12. Knowlton, K. U., Rockman, H. A., Itani, M., Vovan, A., Seidman, C. E., and Chien, K. R. (1995) Divergent pathways mediate the induction of ANF transgenes in neonatal and hypertrophic ventricular myocardium. *J. Clin. Invest.* **96,** 1311–1318
13. Small, E. M., and Krieg, P. A. (2003) Transgenic analysis of the atrialnatriuretic factor (ANF) promoter: Nkx2-5 and GATA-4 binding sites are required for atrial specific expression of ANF. *Dev. Biol.* **261,** 116–131
14. Warren, S. A., Terada, R., Briggs, L. E., Cole-Jeffrey, C. T., Chien, W. M., Seki, T., Weinberg, E. O., Yang, T. P., Chin, M. T., Bungert, J., and Kasahara, H. (2011) Differential role of Nkx2-5 in activation of the atrial natriuretic factor gene in the developing versus failing heart. *Mol. Cell. Biol.* **31,** 4633–4645
15. Simpson, P., McGrath, A., and Savion, S. (1982) Myocyte hypertrophy in neonatal rat heart cultures and its regulation by serum and by catecholamines. *Circ. Res.* **51,** 787–801
16. Siepel, A., Bejerano, G., Pedersen, J. S., Hinrichs, A. S., Hou, M., Rosenbloom, K., Clawson, H., Spieth, J., Hillier, L. W., Richards, S., Weinstock, G. M., Wilson, R. K., Gibbs, R. A., Kent, W. J., Miller, W., and Haussler, D. (2005) Evolutionarily conserved elements in vertebrate, insect, worm, and yeast genomes. *Genome Res.* **15,** 1034–1050
17. Blanchette, M., Kent, W. J., Riemer, C., Elnitski, L., Smit, A. F., Roskin, K. M., Baertsch, R., Rosenbloom, K., Clawson, H., Green, E. D., Haussler, D., and Miller, W. (2004) Aligning multiple genomic sequences with the threaded blockset aligner. *Genome Res.* **14,** 708–715
18. Pollard, K. S., Hubisz, M. J., Rosenbloom, K. R., and Siepel, A. (2010) Detection of nonneutral substitution rates on mammalian phylogenies. *Genome Res.* **20,** 110–121
19. Zhang, Y., Liu, T., Meyer, C. A., Eeckhoute, J., Johnson, D. S., Bernstein, B. E., Nusbaum, C., Myers, R. M., Brown, M., Li, W., and Liu, X. S. (2008) Model-based analysis of ChIP-Seq (MACS). *Genome Biol.* **9,** R137
20. Dekker, J., Rippe, K., Dekker, M., and Kleckner, N. (2002) Capturing chromosome conformation. *Science* **295,** 1306–1311
21. Hagege, H., Klous, P., Braem, C., Splinter, E., Dekker, J., Cathala, G., de Laat, W., and Forne, T. (2007) Quantitative analysis of chromosome conformation capture assays (3C-qPCR). *Nat. Protoc.* **2,** 1722–1733
22. Liao, Y., Ishikura, F., Beppu, S., Asakura, M., Takashima, S., Asanuma, H., Sanada, S., Kim, J., Ogita, H., Kuzuya, T., Node, K., Kitakaze, M., and Hori, M. (2002) Echocardiographic assessment of LV hypertrophy and function in aortic-banded mice: necropsy validation. *Am. J. Physiol. Heart Circ. Physiol.* **282,** H1703–H1708
23. Saadane, N., Alpert, L., and Chalifour, L. E. (1999) Expression of immediate early genes, GATA-4, and Nkx-2.5 in adrenergic-induced cardiac hypertrophy and during regression in adult mice. *Brit. J. Pharmacol.* **127,** 1165–1176
24. Vecchione, C., Fratta, L., Rizzoni, D., Notte, A., Poulet, R., Porteri, E., Frati, G., Guelfi, D., Trimarco, V., Mulvany, M. J., Agabiti-Rosei, E., Trimarco, B., Cotecchia, S., and Lembo, G. (2002) Cardiovascular influences of α1β-adrenergic receptor defect in mice. *Circulation* **105,** 1700–1707
25. Nobrega, M. A., Ovcharenko, I., Afzal, V., and Rubin, E. M. (2003) Scanning human gene deserts for long-range enhancers. *Science* **302,** 413
26. Thomas, J. W., Touchman, J. W., Blakesley, R. W., Bouffard, G. G., Beckstrom-Sternberg, S. M., Margulies, E. H., Blanchette, M., Siepel, A. C., Thomas, P. J., McDowell, J. C., Maskeri, B., Hansen, N. F., Schwartz, M. S., Weber, R. J., Kent, W. J.,

Karolchik, D., Bruen, T. C., Bevan, R., Cutler, D. J., Schwartz, S., Elnitski, L., Idol, J. R., Prasad, A. B., Lee-Lin, S. Q., Maduro, V. V., Summers, T. J., Portnoy, M. E., Dietrich, N. L., Akhter, N., Ayele, K., Benjamin, B., Cariaga, K., Brinkley, C. P., Brooks, S. Y., Granite, S., Guan, X., Gupta, J., Haghighi, P., Ho, S. L., Huang, M. C., Karlins, E., Laric, P. L., Legaspi, R., Lim, M. J., Maduro, Q. L., Masiello, C. A., Mastrian, S. D., McCloskey, J. C., Pearson, R., Stantripop, S., Tiongson, E. E., Tran, J. T., Tsurgeon, C., Vogt, J. L., Walker, M. A., Wetherby, K. D., Wiggins, L. S., Young, A. C., Zhang, L. H., Osoegawa, K., Zhu, B., Zhao, B., Shu, C. L., De Jong, P. J., Lawrence, C. E., Smit, A. F., Chakravarti, A., Haussler, D., Green, P., Miller, W., and Green, E. D. (2003) Comparative analyses of multi-species sequences from targeted genomic regions. *Nature* **424,** 788–793

27. Woolfe, A., Goodson, M., Goode, D. K., Snell, P., McEwen, G. K., Vavouri, T., Smith, S. F., North, P., Callaway, H., Kelly, K., Walter, K., Abnizova, I., Gilks, W., Edwards, Y. J., Cooke, J. E., and Elgar, G. (2005) Highly conserved non-coding sequences are associated with vertebrate development. *PLoS Biol.* **3,** e7
28. Bell, A. C., West, A. G., and Felsenfeld, G. (1999) The protein CTCF is required for the enhancer blocking activity of vertebrate insulators. *Cell* **98,** 387–396
29. Felsenfeld, G., Burgess-Beusse, B., Farrell, C., Gaszner, M., Ghirlando, R., Huang, S., Jin, C., Litt, M., Magdinier, F., Mutskov, V., Nakatani, Y., Tagami, H., West, A., and Yusufzai, T. (2004) Chromatin boundaries and chromatin domains. *Cold Spring Harb. Symp. Quant. Biol.* **69,** 245–250
30. Shen, Y., Yue, F., McCleary, D. F., Ye, Z., Edsall, L., Kuan, S., Wagner, U., Dixon, J., Lee, L., Lobanenkov, V. V., and Ren, B. (2012) A map of the cis-regulatory sequences in the mouse genome. *Nature* **488,** 116–120
31. Birney, E., Stamatoyannopoulos, J. A., Dutta, A., Guigo, R., Gingeras, T. R., Margulies, E. H., Weng, Z., Snyder, M., Dermitzakis, E. T., Thurman, R. E., Kuehn, M. S., Taylor, C. M., Neph, S., Koch, C. M., Asthana, S., Malhotra, A., Adzhubei, I., Greenbaum, J. A., Andrews, R. M., Flicek, P., Boyle, P. J., Cao, H., Carter, N. P., Clelland, G. K., Davis, S., Day, N., Dhami, P., Dillon, S. C., Dorschner, M. O., Fiegler, H., Giresi, P. G., Goldy, J., Hawrylycz, M., Haydock, A., Humbert, R., James, K. D., Johnson, B. E., Johnson, E. M., Frum, T. T., Rosenzweig, E. R., Karnani, N., Lee, K., Lefebvre, G. C., Navas, P. A., Neri, F., Parker, S. C., Sabo, P. J., Sandstrom, R., Shafer, A., Vetrie, D., Weaver, M., Wilcox, S., Yu, M., Collins, F. S., Dekker, J., Lieb, J. D., Tullius, T. D., Crawford, G. E., Sunyaev, S., Noble, W. S., Dunham, I., Denoeud, F., Reymond, A., Kapranov, P., Rozowsky, J., Zheng, D., Castelo, R., Frankish, A., Harrow, J., Ghosh, S., Sandelin, A., Hofacker, I. L., Baertsch, R., Keefe, D., Dike, S., Cheng, J., Hirsch, H. A., Sekinger, E. A., Lagarde, J., Abril, J. F., Shahab, A., Flamm, C., Fried, C., Hackermuller, J., Hertel, J., Lindemeyer, M., Missal, K., Tanzer, A., Washietl, S., Korbel, J., Emanuelsson, O., Pedersen, J. S., Holroyd, N., Taylor, R., Swarbreck, D., Matthews, N., Dickson, M. C., Thomas, D. J., Weirauch, M. T., Gilbert, J., Drenkow, J., Bell, I., Zhao, X., Srinivasan, K. G., Sung, W. K., Ooi, H. S., Chiu, K. P., Foissac, S., Alioto, T., Brent, M., Pachter, L., Tress, M. L., Valencia, A., Choo, S. W., Choo, C. Y., Ucla, C., Manzano, C., Wyss, C., Cheung, E., Clark, T. G., Brown, J. B., Ganesh, M., Patel, S., Tammana, H., Chrast, J., Henrichsen, C. N., Kai, C., Kawai, J., Nagalakshmi, U., Wu, J., Lian, Z., Lian, J., Newburger, P., Zhang, X., Bickel, P., Mattick, J. S., Carninci, P., Hayashizaki, Y., Weissman, S., Hubbard, T., Myers, R. M., Rogers, J., Stadler, P. F., Lowe, T. M., Wei, C. L., Ruan, Y., Struhl, K., Gerstein, M., Antonarakis, S. E., Fu, Y., Green, E. D., Karaoz, U., Siepel, A., Taylor, J., Liefer, L. A., Wetterstrand, K. A., Good, P. J., Feingold, E. A., Guyer, M. S., Cooper, G. M., Asimenos, G., Dewey, C. N., Hou, M., Nikolaev, S., Montoya-Burgos, J. I., Loytynoja, A., Whelan, S., Pardi, F., Massingham, T., Huang, H., Zhang, N. R., Holmes, I., Mullikin, J. C., Ureta-Vidal, A., Paten, B., Seringhaus, M., Church, D., Rosenbloom, K., Kent, W. J., Stone, E. A., Batzoglou, S., Goldman, N., Hardison, R. C., Haussler, D., Miller, W., Sidow, A., Trinklein, N. D., Zhang, Z. D., Barrera, L., Stuart, R., King, D. C., Ameur, A., Enroth, S., Bieda, M. C., Kim, J., Bhinge, A. A., Jiang, N., Liu, J., Yao, F., Vega, V. B., Lee, C. W., Ng, P., Shahab, A., Yang, A., Moqtaderi, Z., Zhu, Z., Xu, X., Squazzo, S., Oberley, M. J., Inman, D., Singer, M. A., Richmond, T. A., Munn, K. J., Rada-Iglesias, A., Wallerman, O., Komorowski, J., Fowler, J. C., Couttet, P., Bruce, A. W., Dovey, O. M., Ellis, P. D., Langford, C. F., Nix, D. A., Euskirchen, G., Hartman, S., Urban, A. E., Kraus, P., Van Calcar, S., Heintzman, N., Kim, T. H., Wang, K., Qu, C., Hon, G., Luna, R., Glass, C. K., Rosenfeld, M. G., Aldred, S. F., Cooper, S. J., Halees, A., Lin, J. M., Shulha, H. P., Zhang, X., Xu, M., Haidar, J. N., Yu, Y., Ruan, Y., Iyer, V. R., Green, R. D., Wadelius, C., Farnham, P. J., Ren, B., Harte, R. A., Hinrichs, A. S., Trumbower, H., Clawson, H., Hillman-Jackson, J., Zweig, A. S., Smith, K., Thakkapallayil, A., Barber, G., Kuhn, R. M., Karolchik, D., Armengol, L., Bird, C. P., de Bakker, P. I., Kern, A. D., Lopez-Bigas, N., Martin, J. D., Stranger, B. E., Woodroffe, A., Davydov, E., Dimas, A., Eyras, E., Hallgrimsdottir, I. B., Huppert, J., Zody, M. C., Abecasis, G. R., Estivill, X., Bouffard, G. G., Guan, X., Hansen, N. F., Idol, J. R., Maduro, V. V., Maskeri, B., McDowell, J. C., Park, M., Thomas, P. J., Young, A. C., Blakesley, R. W., Muzny, D. M., Sodergren, E., Wheeler, D. A., Worley, K. C., Jiang, H., Weinstock, G. M., Gibbs, R. A., Graves, T., Fulton, R., Mardis, E. R., Wilson, R. K., Clamp, M., Cuff, J., Gnerre, S., Jaffe, D. B., Chang, J. L., Lindblad-Toh, K., Lander, E. S., Koriabine, M., Nefedov, M., Osoegawa, K., Yoshinaga, Y., Zhu, B., and de Jong, P. J. (2007) Identification and analysis of functional elements in 1% of the human genome by the ENCODE pilot project. *Nature* **447,** 799–816
32. Blow, M. J., McCulley, D. J., Li, Z., Zhang, T., Akiyama, J. A., Holt, A., Plajzer-Frick, I., Shoukry, M., Wright, C., Chen, F., Afzal, V., Bristow, J., Ren, B., Black, B. L., Rubin, E. M., Visel, A., and Pennacchio, L. A. (2010) ChIP-Seq identification of weakly conserved heart enhancers. *Nat. Genet.* **42,** 806–810
33. Koch, F., Jourquin, F., Ferrier, P., and Andrau, J. C. (2008) Genome-wide RNA polymerase II: not genes only!. *Trends Biochem. Sci.* **33,** 265–273
34. Szutorisz, H., Dillon, N., and Tora, L. (2005) The role of enhancers as centres for general transcription factor recruitment. *Trends Biochem. Sci.* **30,** 593–599
35. Sei, C. A., Irons, C. E., Sprenkle, A. B., McDonough, P. M., Brown, J. H., and Glembotski, C. C. (1991) The α-adrenergic stimulation of atrial natriuretic factor expression in cardiac myocytes requires calcium influx, protein kinase C, and calmodulin-regulated pathways. *J. Biol. Chem.* **266,** 15910–15916
36. Iaccarino, G., Dolber, P. C., Lefkowitz, R. J., and Koch, W. J. (1999) Bβ-adrenergic receptor kinase-1 levels in catecholamine-induced myocardial hypertrophy: regulation by beta- but not alpha1-adrenergic stimulation. *Hypertension* **33,** 396–401
37. Seidman, C. E., Wong, D. W., Jarcho, J. A., Bloch, K. D., and Seidman, J. G. (1988) *Cis*-acting sequences that modulate atrial natriuretic factor gene expression. *Proc. Natl. Acad. Sci. U. S. A.* **85,** 4104–4108
38. Thuerauf, D. J., and Glembotski, C. C. (1997) Differential effects of protein kinase C, Ras, and Raf-1 kinase on the induction of the cardiac B-type natriuretic peptide gene through a critical promoter-proximal M-CAT element. *J. Biol. Chem.* **272,** 7464–7472

Received for publication November 12, 2013.
Accepted for publication January 2, 2014.

Am J Physiol Heart Circ Physiol 307: H1339–H1352, 2014.
First published August 29, 2014; doi:10.1152/ajpheart.01021.2013.

Effects of methylglyoxal on human cardiac fibroblast: roles of transient receptor potential ankyrin 1 (TRPA1) channels

Gaku Oguri,[1] Toshiaki Nakajima,[2] Yumiko Yamamoto,[1] Nami Takano,[1] Tomofumi Tanaka,[1] Hironobu Kikuchi,[1] Toshihiro Morita,[2] Fumitaka Nakamura,[4] Tatsuya Yamasoba,[3] and Issei Komuro[1]

[1]*Department of Cardiovascular Medicine, University of Tokyo, Tokyo, Japan;* [2]*Department of Ischemic Circulatory Physiology, University of Tokyo, Tokyo, Japan;* [3]*Department of Otolaryngology, University of Tokyo, Tokyo, Japan; and* [4]*Teikyo University Chiba Medical Center, Ichihara, Chiba, Japan*

Submitted 28 December 2013; accepted in final form 6 August 2014

Oguri G, Nakajima T, Yamamoto Y, Takano N, Tanaka T, Kikuchi H, Morita T, Nakamura F, Yamasoba T, Komuro I. Effects of methylglyoxal on human cardiac fibroblast: roles of transient receptor potential ankyrin 1 (TRPA1) channels. *Am J Physiol Heart Circ Physiol* 307: H1339–H1352, 2014. First published August 29, 2014; doi:10.1152/ajpheart.01021.2013.—Cardiac fibroblasts contribute to the pathogenesis of cardiac remodeling. Methylglyoxal (MG) is an endogenous carbonyl compound produced under hyperglycemic conditions, which may play a role in the development of pathophysiological conditions including diabetic cardiomyopathy. However, the mechanism by which this occurs and the molecular targets of MG are unclear. We investigated the effects of MG on Ca^{2+} signals, its underlying mechanism, and cell cycle progression/cell differentiation in human cardiac fibroblasts. The conventional and quantitative real-time RT-PCR, Western blot, immunocytochemical analysis, and intracellular Ca^{2+} concentration $[Ca^{2+}]i$ measurement were applied. Cell cycle progression was assessed using the fluorescence activated cell sorting. MG induced Ca^{2+} entry concentration dependently. Ruthenium red (RR), a general cation channel blocker, and HC030031, a selective transient receptor potential ankyrin 1 (TRPA1) antagonist, inhibited MG-induced Ca^{2+} entry. Treatment with aminoguanidine, a MG scavenger, also inhibited it. Allyl isothiocyanate, a selective TRPA1 agonist, increased Ca^{2+} entry. The use of small interfering RNA to knock down TRPA1 reduced the MG-induced Ca^{2+} entry as well as TRPA1 mRNA expression. The quantitative real-time RT-PCR analysis showed the prominent existence of TRPA1 mRNA. Expression of TRPA1 protein was confirmed by Western blotting and immunocytochemical analyses. MG promoted cell cycle progression from G0/G1 to S/G2/M, which was suppressed by HC030031 or RR. MG also enhanced α-smooth muscle actin expression. The present results suggest that methylglyoxal activates TRPA1 and promotes cell cycle progression and differentiation in human cardiac fibroblasts. MG might participate the development of pathophysiological conditions including diabetic cardiomyopathy via activation of TRPA1.

human cardiac fibroblast; transient receptor potential ankyrin 1 channels; methylglyoxal

CARDIAC FIBROBLASTS ARE THE predominant secretary cell types located within the extracellular matrix (ECM) (18), which account for 60~70% of the cells in human hearts and play a key role in regulating normal myocardial function and in the adverse myocardial remodeling that occurs with hypertension, heart failure, and myocardial infarction (12, 71). Many of the functional effects of cardiac fibroblasts are mediated through differentiation of cardiac fibroblasts to myofibroblasts phenotype that expresses contractile proteins such as α-smooth muscle actin (α-SMA), and they consequently exhibit increased migratory and proliferative properties. Cardiac fibroblasts also take a part in the maintenance of myocardial function by producing the type I and type III collagens and by secreting growth factors (48), and a key source of components of the ECM that regulates the structure of the heart and hence mechanical, chemical, and electrical signals between cellular and noncellular components (54). Thus cardiac fibroblasts play an essential role in the fibrosis and remodeling by increased proliferation (4) and elevated collagen production (61) under the various pathophysiological conditions such as diabetic cardiomyopathy (41).

Methylglyoxal (MG) is a highly reactive dicarbonyl metabolite produced during glucose metabolism (23). MG levels mediate rapid nonenzymatic glycation of proteins and other substrates, promoting formation of advanced glycation end (AGE) products, which are involved in the pathogenesis of vascular complications of diabetes (7), (23). AGEs and AGEs receptor (RAGE) cause inflammation, apoptosis, oxidative stress, gene transcription, atherogenesis, and impaired angiogenesis. In addition, MG can react with and modifies certain proteins, lipids, and DNA and alters their normal structure and/or function (7, 23). It has been reported that MG levels were elevated in spontaneously hypertensive rats (68) and in diabetic patients (65) since hyperglycemia strongly enhances MG accumulation (8, 45). In vitro studies also showed that incubation of vascular smooth muscle cells (VSMCs) with high glucose or fructose for 3 h increased MG production 3.5- or 3.9-fold, respectively, and increased oxidative stress (24).

Diabetic cardiomyopathy is a diabetic complication and a risk of heart failure (HF) (10) defined as ventricular dysfunction that occurs in diabetic patients independent of a recognized cause (e.g., coronary heart disease, hypertension). Diastolic dysfunction is a functional character in diabetic cardiomyopathy (27), (57). AGE product deposition has been reported to increase LV diastolic stiffness directly by cross-linking collagen, indirectly by enhancing collagen formation or reducing nitric oxide bioavailability (33, 63). Recently, Shao et al. (56) showed that MG reduced the ability of sarco(endo) plasmic reticulum Ca^{2+}-ATPase 2a to transport Ca^{2+} and induced diastolic dysfunction, which may play a role in development of diabetic cardiomyopathy. In addition, MG has been reported to affect cardiac fibroblasts function by promoting myofibroblast differentiation (74), but the mechanism by which this occurs and the molecular targets of MG are unclear.

The transient receptor potential (TRP) channel superfamily consists of 28 mammalian cation channels and is expressed in

Address for reprint requests and other correspondence: T. Nakajima, Dept. of Ischemic Circulatory Physiology, Univ. of Tokyo, 7-3-1 Hongo, Bunkyo-ku, Tokyo, Japan (e-mail: nakajima-2im@h.u-tokyo.ac.jp).

almost tissue, including the heart. Most TRP channels are permeable to Ca^{2+} and are prime molecular candidates for store-operated channels, receptor-operated channels, ligand-gated channels, and stretch-activated channels. In the whole heart, the expression of several TRP channels has been demonstrated in RT-PCR or biochemical studies (31, 36). These TRP channels act as multifunctional cellular sensors and have several fundamental cell functions such as contraction, proliferation, and secretion. Among TRP channel family, several studies have revealed the involvement of TRP channels (TRPCs) on cardiac hypertrophy and remodeling (31, 44, 72). Cardiac fibroblasts also contribute to the pathogenesis of cardiac remodeling, and the existence of TRPC1, 3, 4, and 6 has been reported by RT-PCR analysis in cardiac fibroblasts (17, 25, 35). Treatment with TGF-β1 has been reported to increase the Ca^{2+} influx via activation of TRP channels (TRPM7, TRPC1, and TRPC6) (25, 35). Davis et al. (22) showed an obligate function for TRPC6 in promoting myofibroblast differentiation and wound healing in mice, whereas Harada et al. (32) reported the essential role of TRPC3 on rat cardiac fibroblast proliferation and differentiation. The function and existence of TRPV1, TRPV2, and TRPV4 have also been reported in cardiac fibroblasts and myocytes (34, 42, 75).

Alternatively, the TRP ankyrin channel (TRPA) is also a member of the large TRP family of ion channels and functions as a Ca^{2+} permeable nonselective cation channel. The only mammalian TRPA subfamily member, TRPA1, is widely expressed in peripheral and central termini of small diameter primary afferent neurons and the ganglia of these dorsal, trigeminal, and nodose neurons (6, 59), and nonneuronal cells including epithelial cells (49). Based on localization and functional properties, TRPA1 is considered a key player in acute and chronic (neuropathic) pain and inflammation and integrates the nociception of a large variety of different, potentially damaging and noxious stimuli: cold (40, 59) and electrophilic compounds (6, 38). Diabetic neuropathy is one of diabetic complication. And it has been reported that a rise in serum MG density participates in diabetic neuropathy directly (9), and MG activates nociceptors through TRPA1 in diabetic neuropathy (26, 53). Thus it is likely that MG may play a role in diabetic complication such as neuropathy. Therefore, it is interesting to investigate the molecular target of MG and involvement of TRPA1 on human cardiac fibroblasts.

The purpose of the present study is to investigate the expression and function of TRPA1 and the effects of MG on Ca^{2+} signals, fibroblast proliferation, and differentiation in human cardiac fibroblasts. We show that MG activates TRPA1 and promotes cell cycle progression and differentiation in human cardiac fibroblasts.

MATERIALS AND METHODS

Cell culture of human cardiac fibroblasts. Human adult ventricular cardiac fibroblasts (ACBRI 5118) were purchased from DS Pharma Biomedical (Osaka, Japan). Cells were maintained at 37°C under 5% CO_2 in Cell System containing 10% serum and defined cell boost (CSC Catalog 4ZO-50). At confluence, the cells were detached using 0.25% trypsin in 0.02% EDTA and cultured into the medium. Medium was replaced more than twice weekly. Cells before confluence at passage 3–6 were detached from culture dish with 0.25% trypsin in 0.02% EDTA and used for later experiments.

Solutions and drugs. MG was purchased from Nakarai Tesque (Kyoto, Japan). HC030031 [2-(1,3-dimethyl-2,6-dioxo-1,2,3,6-tetrahydro-7H-purin-7-yl)-N-(4-isopropylphenyl)acetamide], a selective TRPA1 blocker, was purchased from Abcam Biochemicals (Cambridge, UK). Ruthenium red, a general cation channel blocker, and allyl isothiocyanate (AITC), a selective TRPA1 agonist (38), and 15-deoxy-delta-12, 14-prostaglandin J2 (15d-PGJ2) were purchased from Wako Pure Chemical Industries (Osaka, Japan). Nicardipine, aminoguanidine, dithiothreitol (DTT), and fura-2 acetoxymethyl ester (fura-2 AM) were purchased from Sigma-Aldrich (Poole, UK). LY2157299, a potent and selective TGF-β_1 receptor blocker, was purchased from AdooQ BioScience.

Measurement of intracellular Ca^{2+} concentration $[Ca^{2+}]_i$. Cytosolic free Ca^{2+} concentration ($[Ca^{2+}]_i$) was determined using the fluorescence method as described previously (30, 52). Human cardiac fibroblasts were trypsinized, washed twice in the standard solution, adjusted to a cell density of 10^6 cells ml-1 and loaded with 2 μM fura-2 AM for 30 min at 37°C under 5% CO_2. After incubation, the medium containing fura-2 AM was removed, and fluorescent cells in suspensions were measured at 37°C while stirred continuously in a cuvette placed by a spectrofluorometer (CAF-100; Jasco, Tokyo, Japan). The excitation wavelengths were 340 and 380 nm, and emission was 500 nm. In the evaluation of Ca^{2+} responses, the amplitude of Ca^{2+} elevation in response to each stimulant was calculated by the increase of F340/F380 with reference to the value at the resting state. In experiments of HC030031, ruthenium red, or DTT, we added them 1 min before the application of Ca^{2+} into the bath solution.

Immunocytochemistry. Immunocytochemistry was performed on human cardiac fibroblasts using anti-TRPA1 channels antibodies (Novus Biologicals) or anti-α-smooth muscle actin (SMA) (Cy3-conjugated anti-α-actin; Sigma). The cells were cultured on Lab-Tek collagen-coated chamber slide (Nalge Nunc International, Naperville, IL), fixed with 2% paraformaldehyde in PBS in 20 min, and then blocked for 15 min with 2% horse serum and 0.1% saponin in PBS. The cells were incubated for 1 h with primary antibodies diluted with 0.01% Triton X and 0.01% NaN3 in PBS into 1:200–1:1,000. For negative controls, cells were treated with normal Rabbit IgG. Alexa Fluor 555 labeled Goat anti-rabbit IgG antibody diluted 1:1,000 (Molecular Probes; A21428) was used to visualize the channel expression. The cells were also stained with 2-(4-amidinophenyl)-1H-indole-6-carboxamidine (DAPI) to visualize nuclei. A confocal laser scanning microscopy (Olympus Fluo View FV300; Olympus) was used for observations.

RNA extraction, RT-PCR, and real-time quantitative RT-PCR. To determine the expression of TRP channel in human cardiac fibroblasts by RT-PCR, total cellular RNA was extracted from the cultured cells by using the RNeasy mini kit (Qiagen, Cambridge, MA). For RT-PCR, complementary DNA (cDNA) was synthesized from 1 μg of total RNA with reverse transcriptase with random primers (Toyobo, Osaka, Japan). The reaction mixture was then subjected to PCR amplification with specific forward and reverse oligonucleotide primers for 35 cycles consisting of heat denaturation, annealing, and extension. The cycling conditions were denaturation at 98°C for 20 s, annealing at 52–56°C for 10 s, and extension at 74°C for 1 min. PCR products were size-fractionated on 2% agarose gels and stained with ethidium bromide and visualized under UV light. The forward and reverse primer sequences for TRPA1 were 5′-TGGTGCACAA-ATAGACCCAGT-3′ and 5′-TGGGCACCTTTAGAGAGTAGC -3′. The forward and reverse primer sequences for GAPDH were 5′-GAGTCAACGGATTTGGTCGT -3′ and 5′-TGACAAAGTGGTC-GTTGAGG -3′.

Real-time quantitative RT-PCR was performed with the use of real-time Taq-Man technology and a sequence detector (ABI PRISM7000; Applied Biosystems, Foster City, CA). Gene-specific primers and Taq-Man probes were used to analyze transcript abundance. The 18S ribosomal RNA level was analyzed as an internal

control and used to normalize the values for transcript abundance of TRP family genes. The probes used in this study ware purchased as Assay-on-Demand from Applied Biosystems (Foster City, CA): assay ID Hs00175798_m1 for TRPA1, assay ID Hs00608195_m1 for TRPC1, assay ID Hs01066071 _m1 for TRM2, assay ID Hs00218912 _m1 for TRPV1, assay ID Hs00901640_m1 for TRPV2, and assay ID 4310893E for 18S rRNA endogenous control.

Western blotting. Proteins were separated on a 10% polyacrylamide gel for 60 min at 200 V and then transferred to Amersham Hypond-P (GE Healthcare UK, Buckinghamshire, England) for 60 min at 72 mA with semi-dry method. After the transfer, the membrane was blocked with Blocking One (Nakarai Tesque, Kyoto, Japan) at room temperature for 1 h. The membrane was then exposed to anti-TRPA1 antibodies (Novus Biologicals, Littleton, CO) or anti-α-SMA (Cy3-conjugated anti-α-actin; Sigma) at the dilutions in blocking buffer overnight at 4°C. Probed membrane was then washed three times in PBS-T for 15 min each time and subsequently incubated with anti-rabbit IgG linked to peroxidase (Santa Cruz Biotechnology) diluted to 1:5,000 with blocking buffer for 1 h at room temperature. After three additional washes, bound antibodies were detected by Chemi-Lumi One Super (Nacalai Tesque, Kyoto, Japan) and analyzed with an LAS-3000 mini image analyzer (Fuji-Film, Tokyo, Japan).

Transfection of synthetic small interfering RNA. TRPA1 small interfering RNA (siRNA; Sense: ACGAAUUCAUAUCUAA-UAATT; Antisense: UUAUUAGAUAUGAAUUCCGUGG) and nonsilencing siRNA (negative control; Allstars Negative control) were purchased from Qiagen (Cambridge, MA). They were transfected into human cardiac fibroblasts to a final concentration of 24 nmol/l, by using the Lipofectamine RNAiMAX Transfection Reagent (10 ml/ml culture; Life Technologies, Carlsbad, CA) according to the instructions of the manufacturer. Transfected cells were incubated for 48 h in an atmosphere of 5% CO_2 and 95% air at 37°C before each experiment. Analysis of mRNA by using real-time RT-PCR and the functions of the cells were then performed. Rhodamine-conjugated siRNA was used to confirm the transfection of siRNA by using Nikon ECLISE TE200-u.

Cell-cycle analysis using flow cytometry. Human cardiac fibroblasts were plated about 5,000 cells/cm^2 into 6-cm dishes, after saved in serum-free media for 24 h, and in the presence or absence of methylglyoxal (300 μM) or drugs for 48 h at 37°C, 5% CO_2. After 48 h incubation, cells were totally washed in PBS (Wako Pure Chemical Industries, Osaka, Japan) and harvested from all dishes following trypsinization. Cells were then mixed in 500 μl of PBS contained 3% FBS and 0.05% NaN_3 and centrifuged. And cells were added 5 ml of ice-cold 70% ethanol and resuspended and incubated at room temperature for 30 min. They were then again centrifuged and added PBS contained 0.05 mg/ml Ribonuclease A (Sigma-Aldrich) and 0.01 mg/ml propidium iodide (PI; Sigma-Aldrich). The final volume in each sample was 600 μl. In each preparation, the numbers of cells and PI fluorescence were measured with a Guva easycyteplus (Merck Millipore, Billerica, MA) at 680 nm emission-wavelength to create a DNA content-frequency histogram. Samples were gated on fibroblast population stained PI. The percentage of cells in each phase of the cell cycle, G0/G1, S, and G2/M phases, was analyzed using Cytosoft 5.3 of Merck Millipore.

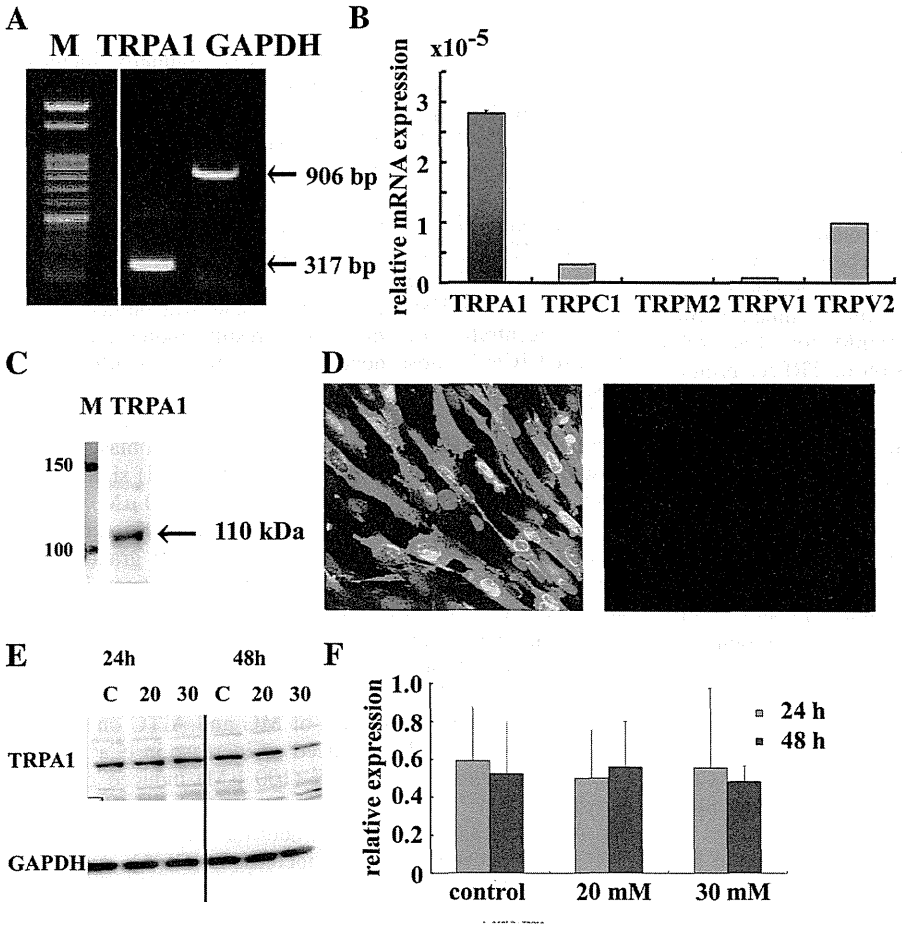

Fig. 1. Transient receptor potential ankyrin 1 (TRPA1) expression in human cardiac fibroblasts. *A*: expression of α subunit gene of TRPA1 channel in human cardiac fibroblasts. Marker, M; GAPDH, used as a loading control. *B*: quantitative real-time RT-PCR analysis of TRPA1, TRPC1, TRPM2, TRPV1, and TRPV2 in human cardiac fibroblasts. The expression levels of TRP channel genes were normalized to those of the 18S ribosomal RNA levels. Note that dominant expression of TRPA1 mRNA was observed in human cardiac fibroblasts. *C*: Western blotting for TRPA1 (indicated by an arrow). *D*: immunostaining for TRPA1. Negative control without the antibody (right part). Double staining of nuclei DAPI to visualize nuclei is illustrated. Note that human cardiac fibroblasts have significant expression for TRPA1. *E* and *F*: effects of high glucose (20 and 30 mM) on TRPA1 expression. The cells were treated with 5.4 mM (control solution), 20 mM, and 30 mM (high glucose solution) for 24 h and 48 h. The TRPA1 protein expression was measured by Western blotting, and the ratio of TRPA1 optical density to the corresponding GAPDH optical density is shown in *F*. Each data represents the mean ± SD of paired 3 different experiments.

Data analysis. All values are expressed as means ± SD. Differences between groups were compared by one-way ANOVA and Bonferroni's post hoc test. Two-group analysis was performed with a Student's *t*-test. The level of significance was set at $P < 0.05$.

RESULTS

Expression of TRPA1 mRNA in human cardiac fibroblasts. We investigated the expression of TRPA1 in human cardiac fibroblasts (Fig. 1*A*). TRPA1 mRNA was detected in human cardiac fibroblasts. The amplitude of cDNA fragments was of predicted molecular size (317 bp), identical to cDNA fragments amplified from reversely transcripted mRNA.

The expression level of TRPA1 and TRP family mRNA members (TRPC1, TRPM2, TRPV1, and TRPV2) was compared by real-time quantitative RT-PCR analysis (Fig. 1*B*). Transcript levels were normalized to 18S ribosomal housekeeping gene. Significant expression of TRPA1, TRPC1, TRPV1, and TRPV2 mRNA was observed. The relative abundance of TRP mRNA was TRPA1>TRPV2>TRPC1>TRPV1. Thus TRPA1 appears to be dominantly expressed in human cardiac fibroblasts.

Expression of TRPA1 protein in human cardiac fibroblasts (immunocytochemistry and Western blotting). To confirm TRPA1 protein expression, Western blot analysis was performed. A specific antibody for TRPA1 channel protein revealed a strong band as shown in Fig. 1*C*. Expression of TRPA1 was also confirmed by immunocytochemistry in human cardiac fibroblasts as shown in Fig. 1*D*. The cells were also counterstained with DAPI to visualize nuclei, and double staining of nucleus and TRPA1 channel protein. No significant expression was detected in negative controls with normal rabbit IgG instead of a primary antibody (Fig. 1*D*, right part). These Western blotting and immunocytochemical analysis showed the expression of TRPA1 in human cardiac fibroblasts.

It has been reported that high glucose modulates the expression of TRPC such as TRPC6 (29, 73). Therefore, we investigated the effects of high glucose (20 and 30 mM) on TRPA1 expression. As shown in Fig. 1*E*, treatment of human cardiac fibroblasts with high glucose (20 and 30 mM) for 24 and 48 h did not significantly affect the expression of TRPA1 protein, compared with the control solution (5.4 mM glucose).

Effects of MG and AITC on $[Ca^{2+}]_i$ in human cardiac fibroblasts. The above results suggest that the definite expression of TRPA1 was observed in human cardiac fibroblasts. Therefore, to investigate whether TRPA1 can function in cardiac fibroblasts, the $[Ca^{2+}]_i$ measurement using fura-2 AM was applied. The effects of a dicarbonyl compound MG, an agent to activate TRPA1 (13, 26, 53), which is produced during glucose metabolism and in higher levels under hyperglycemic conditions, on $[Ca^{2+}]_i$ were investigated. In the presence of extracellular Ca^{2+}, MG (500 μM) significantly induced an increase of $[Ca^{2+}]_i$ (Fig. 2*A*). In contrast, in a cell bathed into the Ca^{2+}-free standard solution, MG (500 μM; Fig. 2*B*) did not significantly increase $[Ca^{2+}]_i$. These results suggest that MG mainly increased $[Ca^{2+}]_i$ due to Ca^{2+} entry, but not Ca^{2+} release from intracellular store sites in human cardiac fibroblasts.

Figure 3 shows the concentration-dependent effects of MG (10–1,000 μM) on $[Ca^{2+}]_i$. MG significantly increased $[Ca^{2+}]_i$ in a concentration-dependent manner. The application of MG

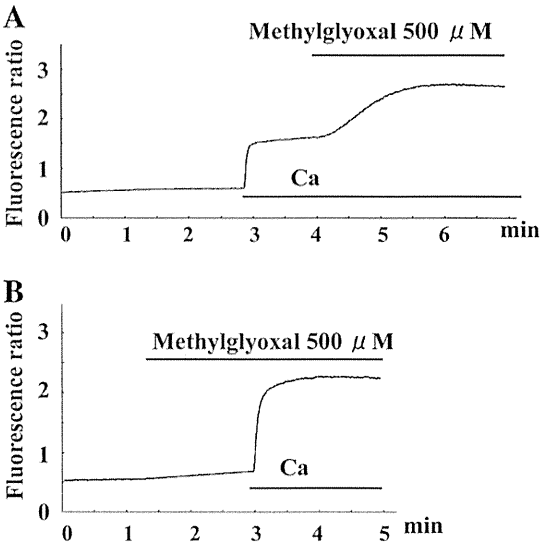

Fig. 2. Effects of methylglyoxal on intracellular Ca^{2+} concentration $[Ca^{2+}]_i$ in human cardiac fibroblasts. The Ca^{2+}-free bathing solution contained 0.9 mM EGTA in the absence of Ca^{2+}. *A* and *B*: effects of methylglyoxal (500 μM) on $[Ca^{2+}]_i$. In the presence of extracellular Ca^{2+}, methyglyoxal (*A*) increased $[Ca^{2+}]_i$. However, methylglyoxal (*B*) did not significantly increased $[Ca^{2+}]_i$ in the Ca^{2+}-free bathing solution, but the additional application of extracellular Ca^{2+} (5 mM) induced an increase of $[Ca^{2+}]_i$.

at concentrations lower than 300 μM gradually increased $[Ca^{2+}]_i$ in a concentration-dependent manner. MG (1,000 μM) induced a biphasic increase of $[Ca^{2+}]_i$. It induced a sharp peak response of $[Ca^{2+}]_i$, followed by a gradual decrease. The decay of $[Ca^{2+}]_i$ during continuous application of MG may be due to the desensitization induced by Ca^{2+} entering the channel (3, 51, 70). Figure 3*B* showed the concentration-dependent effects of MG on $[Ca^{2+}]_i$. The increased value in F340/F380 measured at the peak level or 2 min after the application of MG with reference to F340/F380 at the resting state was plotted against each concentration of MG. These results indicate that MG increased $[Ca^{2+}]_i$ dose dependently in human cardiac fibroblasts.

Figure 4*A* shows the effects of AITC, a selective TRPA1 agonist (38), on $[Ca^{2+}]_i$ in human cardiac fibroblasts. In the presence of extracellular Ca^{2+}, AITC (100 μM) significantly increased $[Ca^{2+}]_i$. The application of AITC (100 μM) induced a biphasic increase of $[Ca^{2+}]_i$ (Fig. 4*A*). The addition of AITC rapidly increased $[Ca^{2+}]_i$, and the $[Ca^{2+}]_i$ rise gradually decreased and reached to the steady state. In contrast, in a cell bathed into the Ca^{2+}-free standard solution, AITC (100 μM) did not significantly increase $[Ca^{2+}]_i$. Similarly, PGJ_2 (Fig. 4*C*, 30 μM), an agent known as other TRPA1 agonist (20), significantly increased $[Ca^{2+}]_i$.

Figure 4*B* shows the effects of MG and AITC on $[Ca^{2+}]_i$. MG (500 μM; Fig. 4*Ba*) induced an increase in $[Ca^{2+}]_i$. The additional application of AITC (100 μM) induced a further increase of $[Ca^{2+}]_i$. On the other hand, after AITC (100 μM; Fig. 4*Bb*) increased $[Ca^{2+}]_i$, the additional application of MG (100 μM) induced a only small increase in $[Ca^{2+}]_i$, suggesting that MG and AITC activated the common Ca^{2+}-influx pathways in human cardiac fibroblasts.

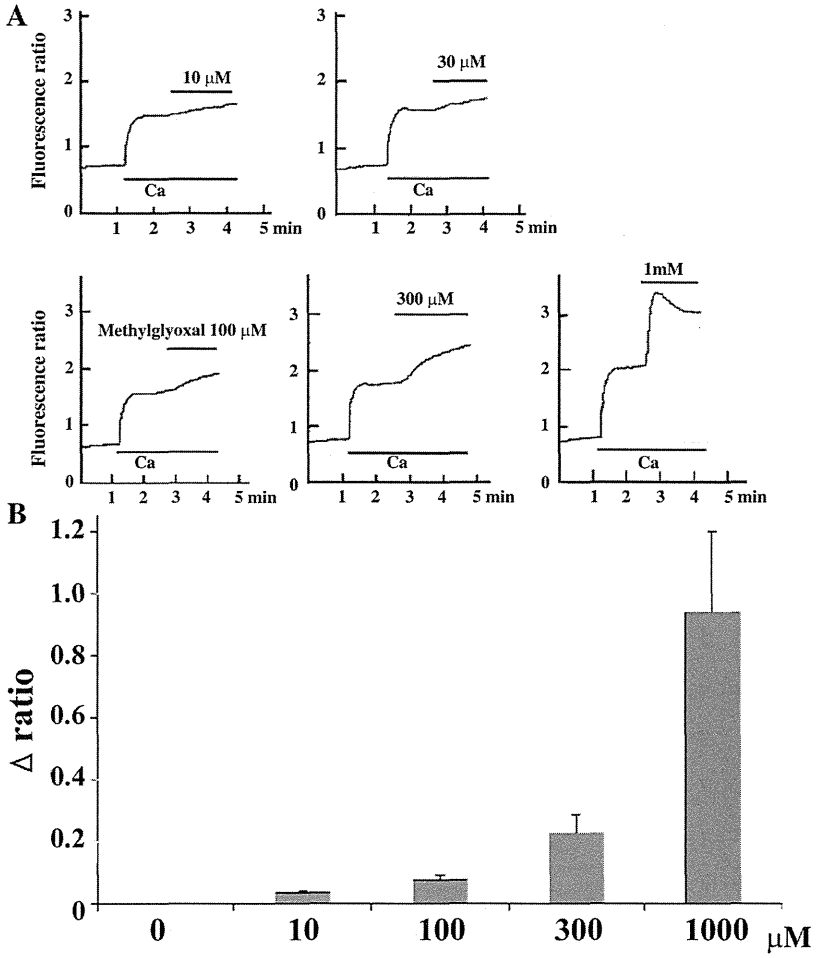

Fig. 3. Dose-dependent effects of methylglyoxal on $[Ca^{2+}]_i$. Concentration-dependent effects of methylglyoxal on $[Ca^{2+}]_i$ are shown. In *A*, the typical original traces are illustrated. The data were representative of 4 different experiments. In *B*, the increased value in F340/F380 measured 2 min after the application of methylglyoxal with reference to F340/F380 at the resting state was plotted against each concentration of methylglyoxal (0, 10, 100, 300, 1,000 μM). Each data represent the mean ± SD of paired 4 different experiments.

Effects of HC030031 and ruthenium red on MG-induced $[Ca^{2+}]_i$ increase. These results suggest the involvement of TRPA1 on MG-induced $[Ca^{2+}]_i$ increase in human cardiac fibroblasts. Therefore, we investigated the effects of HC030031 (50, 100 μM), a selective TRPA1 antagonist, on MG-induced $[Ca^{2+}]_i$ increase. As shown in Fig. 5*A*, HC030031 (100 μM) significantly inhibited the MG-induced $[Ca^{2+}]_i$ increase, compared with control cells, suggesting that TRPA1 is involved in MG-induced $[Ca^{2+}]_i$ increase in human cardiac fibroblasts. HC030031 (100 μM) inhibited MG-induced $[Ca^{2+}]_i$ rise by 71 ± 7% (n = 3; Fig. 5*B*).

Effects of various blockers on MG and AITC-induced $[Ca^{2+}]_i$. We next investigated the effects of various blockers on MG-induced $[Ca^{2+}]_i$ rise. First, we added 10 μM nicardipine, a L-type Ca^{2+} channel blocker, into the cuvette before the addition of extracellular calcium. The inclusion of 10 μM nicardipine in the bath solution did not significantly affect MG-induced Ca^{2+} entry, compared with the control cells (data not shown), suggesting that L-type Ca^{2+} channel does not significantly contribute to the Ca^{2+} influx elicited by MG in human cardiac fibroblasts. Similarly, mibefradil (10 μM), a T-type Ca^{2+} channel blocker, did not affect the $[Ca^{2+}]_i$ rise (data not shown). To further determine the type of channels involved in the calcium influx, the effects of ruthenium red (5, 10 μM), a nonselective TRP blocker including TRPA1, were investigated as shown in Fig. 5, *A* and *C*. Pretreatment with ruthenium red (10 μM; Fig. 5*A*) significantly inhibited MG-induced $[Ca^{2+}]_i$, compared with control cells. Ruthenium red (10 μM) inhibited methylglyoxal-induced $[Ca^{2+}]_i$ rise by 77 ± 11% (n = 4; Fig. 5*C*).

In addition, it is very likely that MG stimulates TRPA1 through formation of reversible hemithioacetals with cysteine residues (26). To investigate this possibility, we examined the effect of the reducing agent, DTT (10 mM), on methylglyoxal-induced $[Ca^{2+}]_i$. As shown in Fig. 5*D*, treatment of DTT (10 mM) inhibited methylglyoxal-induced $[Ca^{2+}]_i$. DTT (10 mM) inhibited MG-induced $[Ca^{2+}]_i$ rise by 81 ± 5% (n = 4; Fig. 5*E*).

Effects of aminoguanidine on MG-induced $[Ca^{2+}]_i$ rise. Figure 6 shows the effects of aminoguanidine, a MG scavenger (46, 67), on MG-induced $[Ca^{2+}]_i$ rise. The cells were pretreated with various concentrations of aminoguanidipne, and then MG was added into the bathing solution. The $[Ca^{2+}]_i$ response was compared with the control cells (untreated cells). Treatment with aminoguanidine (1–10 mM) inhibited MG-induced $[Ca^{2+}]_i$ rise in a concentration-dependent manner as shown in Fig. 6*B*.

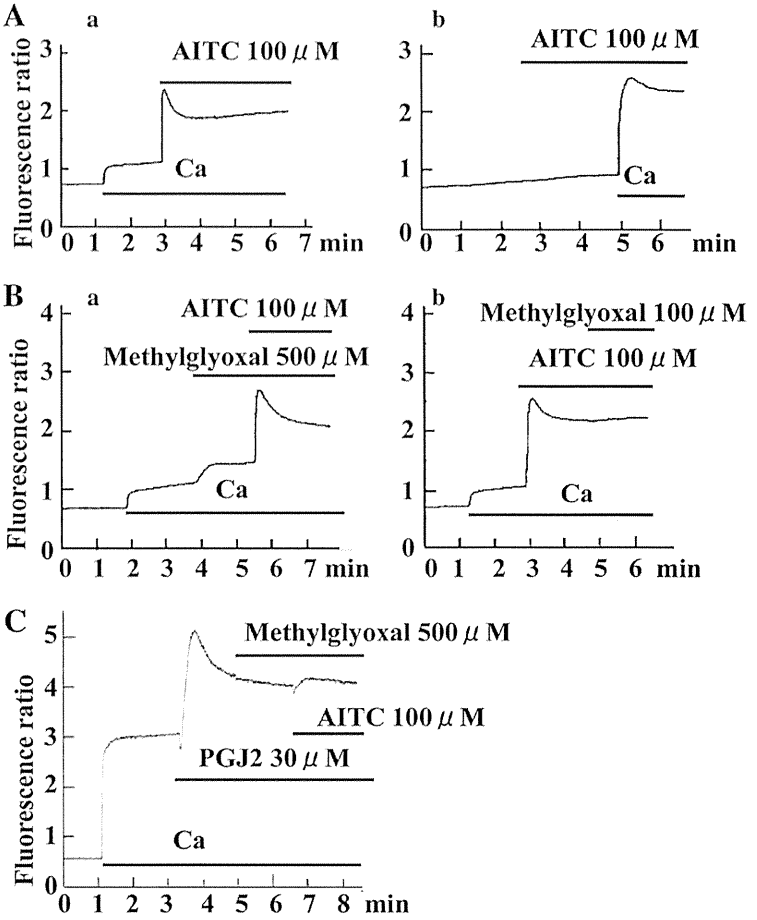

Fig. 4. Effects of methylglyoxal, allyl isothiocyanate (AITC), and PGJ_2 on intracellular Ca^{2+} concentration $[Ca^{2+}]_i$ in human cardiac fibroblasts. The Ca^{2+}-free bathing solution contained 0.9 mM EGTA in the absence of Ca^{2+}. *A*: effects of AITC on $[Ca^{2+}]_i$. In the presence of extracellular Ca^{2+}, AITC (100 μM; *Aa*) increased $[Ca^{2+}]_i$. However, AITC (100 μM; *Ab*) did not significantly increased $[Ca^{2+}]_i$ in the Ca^{2+}-free bathing solution, but the additional application of extracellular Ca^{2+} (5 mM) induced an increase of $[Ca^{2+}]_i$. *B*: effects of methylglyoxal and AITC on $[Ca^{2+}]_i$ in the presence of extracellular Ca^{2+}. Note that after AITC (100 μM; *Ab*) increased $[Ca^{2+}]_i$, the additional application of methylglyoxal induced a only small increase in $[Ca^{2+}]_i$, suggesting that methylglyoxal and AITC activated the same Ca^{2+}-influx pathways. *C*: effects of prostaglandin J2 (PGJ_2; 30 μM) on $[Ca^{2+}]_i$. After PGJ_2 (30 μM) increased $[Ca^{2+}]_i$, the additional application of methylglyoxal and AITC induced a only small increase in $[Ca^{2+}]_i$. The typical data obtained from 4 independent experiments are shown in each trace.

Effects of treatment with siRNA targeted for TRPA1 on expression level of TRPA1 mRNA and MG-induced $[Ca^{2+}]_i$ increase. To determine whether TRPA1 is involved in $[Ca^{2+}]_i$ mobilization induced by MG in human cardiac fibroblasts, we investigated the effects of siRNA targeted for TRPA1. After siRNA transfection, the level of TRPA1 mRNA expression was analyzed by real-time quantitative RT-PCR. The expression level of TRPA1 mRNA in cells transfected with siRNA significantly decreased, compared with nonsilencing (negative control) siRNA-treated cells (Fig. 7*A*). In addition, the MG-induced $[Ca^{2+}]_i$ response was compared in between siRNA- and nonsilencing (negative control) siRNA-treated cells. MG-induced $[Ca^{2+}]_i$ rise was significantly inhibited in cells transfected with siRNA for TRPA1 (Fig. 7, *B* and *C*), compared with nonsilencing (negative control) siRNA-treated cells. These results suggest that TRPA1 is mainly involved in MG-induced calcium entry from extracellular medium in human cardiac fibroblasts.

Effects of MG on cell cycle progression in human cardiac fibroblasts. We investigated the effects of MG on cell cycle. Cells were treated in the absence or presence of MG (300 μM) for 48 h and analyzed by flow cytometry. Treatment with MG (300 μM; Fig. 8) showed a larger proportion of cells entering G2/M and a smaller proportion arrested in G0/G1, compared with control cells. These results suggest that MG induced cell proliferation with cell cycle progression to S and G2/M.

Figures 9 and 10 show the effects of ruthenium red (Fig. 9, 10 μM) and HC030031 (Fig. 10, 100 μM) on MG-induced cell cycle progression in human cardiac fibroblast. Treatment with ruthenium red (Fig. 9) and HC030031 (Fig. 10) inhibited MG-induced cell cycle entry/progression with a smaller proportion of cells entering S and G2/M and a larger proportion arrested in G0/G1.

Effects of MG on cell differentiation. After fibroblasts proliferate, they differentiate into ECM proteins -secreting myofibroblasts characterized by altered morphology and increased α-SMA expression. The effects of MG on α-SMA protein expression were investigated as shown in Fig. 11. Treatment with MG (30–300 μM) for 24 h enhanced α-SMA expression as shown in Western blotting (Fig. 11, *A* and *B*). The significant staining of α-SMA was observed in cells treated with MG for 24 h (Fig. 11*C*), compared with negative control.

Figure 12, *A* and *B*, shows the effects of ruthenium red (10 μM) and HC030031 (100 μM) on MG-enhanced α-SMA expression. Treatment with MG (300 μM) enhanced α-SMA protein expression, and ruthenium red and HC030031 significantly inhibited MG-enhanced α-SMA expression as shown in Fig. 12*B*.

MG enhances α-SMA expression by a TGF-β_1-independent mechanism. To investigate whether MG enhances α-SMA expression independently of TGF-β_1, we have performed the following experiments. First, TGF-β_1 levels were evaluated by

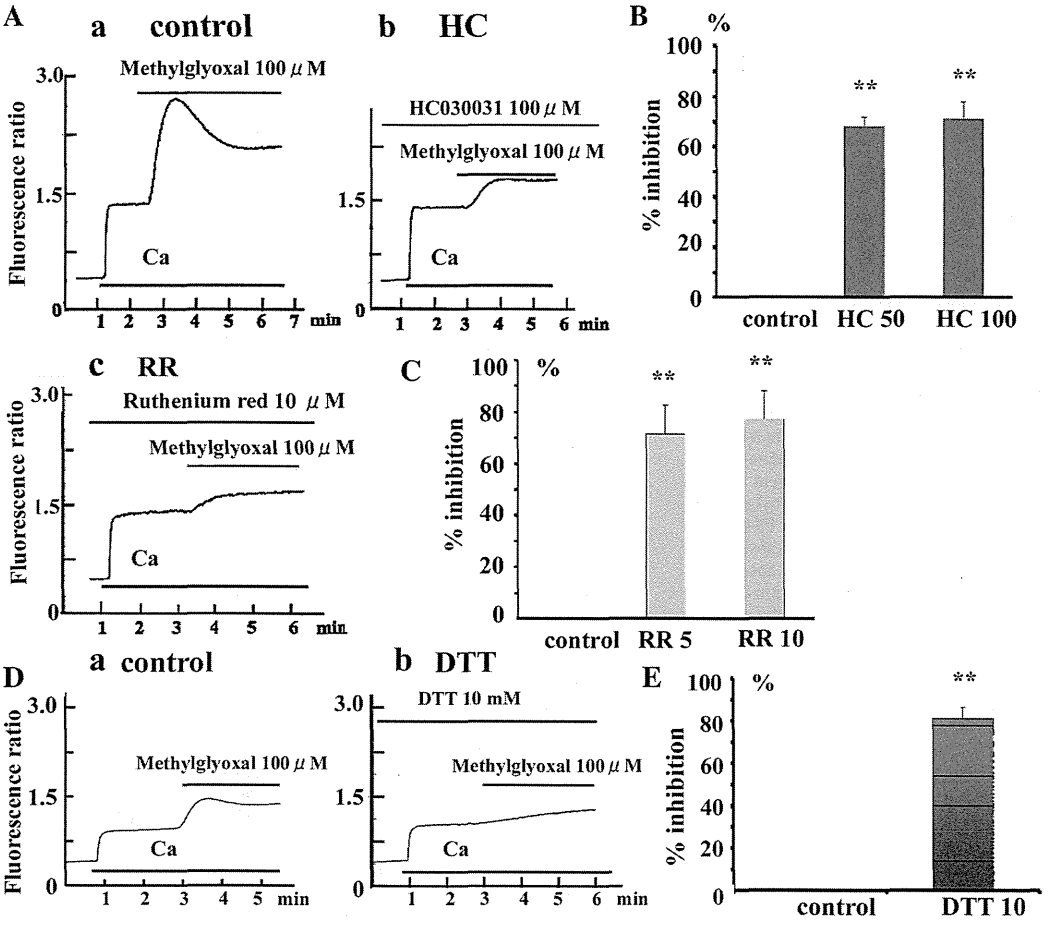

Fig. 5. Effects of HC030031, ruthenium red (RR), and DTT on methylglyoxal-induced $[Ca^{2+}]_i$ entry. Effects of HC030031 (*A* and *B*) and RR (*A* and *C*) on methylglyoxal-induced $[Ca^{2+}]_i$ rise. The cells were pretreated with these agents, and then methylglyoxal was added into the bathing solution. The $[Ca^{2+}]_i$ response was compared with the control cells (untreated cells). The typical data are illustrated in *A*. *Aa*: control cells. *Ab*: HC030031 (100 μM)-treated cells. *Ac*: RR (10 μM)-treated cells. The data were representative of 4 different experiments. *B* and *C*: inhibitory effects of HC030031 (*B*; 50 and 100 μM) and RR (*C*; 5 and 10 μM) on methylglyoxal-$[Ca^{2+}]_i$ rise. The increased value in F340/F380 induced by methylglyoxal was obtained in the absence or presence of drugs. The increased value in the absence of drugs is considered as 100%. The percent inhibition of these agents is illustrated in *B* and *C*. *D* and *E*: effects of DTT on methylglyoxal-$[Ca^{2+}]_i$ rise. The cells were pretreated with DTT for 1 min. Each datum represents the mean ± SD of paired 4 different experiments. $^{**}P <$ 0.01 vs. control.

ELISA in conditioned media from MG-treated cells. Treatment of MG (300 μM) for 24 h did not significantly increase TGF-β_1 production. The concentration of TGF-β in bath solution was 34.9 ± 29.5 (in pg/ml; n = 8) in control, 34.1 ± 25.8 (in pg/ml; n = 8) in cells bathed with MG (30 μM) for 24 h, and 28.2 ± 19.9 (in pg/ml; n = 8) in cells bathed with MG (300 μM) for 24 h, suggesting that treatment with MG for 24 h did not enhance TGF-β_1 secretion in the present conditions. In addition, LY2157299 (0.1 and 1 μM), a potent and selective TGF-β_1 receptor blocker, did not inhibit the MG-enhanced α-SMA expression as shown in Fig. 12, *C* and *D*. These results suggest that MG enhanced α-SMA expression independently of endogenous TGF-β_1 production or activation.

DISCUSSION

The major findings of the present study are as follows. First, in human cardiac fibroblasts, MG induced Ca^{2+} entry in a concentration-dependent manner. Second, treatment with ruthenium red (RR), a general cation channel blocker, and HC030031, a selective transient receptor potential ankyrin 1 (TRPA1) antagonist, inhibited MG-induced Ca^{2+} entry. Treatment with an MG scavenger, aminoguanidine, and DTT, a reducing agent, also antagonized it. Third, AITC, a selective TRPA1 agonist, increased induced Ca^{2+} entry. The use of siRNA to knock down TRPA1 markedly reduced the MG-induced Ca^{2+} entry as well as the expression level of TRPA1 mRNA. Fourth, the conventional and quantitative real-time RT-PCR analysis showed the prominent existence of TRPA1 mRNA. Expression of TRPA1 protein was confirmed by Western blotting and immunocytochemical analyses. Finally, MG promoted cell cycle progression from G0/G1 to S/G2/M, which was significantly suppressed by treatment with HC030031 or RR. MG also enhanced α-SMA expression. The present results suggest that MG activates TRPA1 and promotes cell cycle

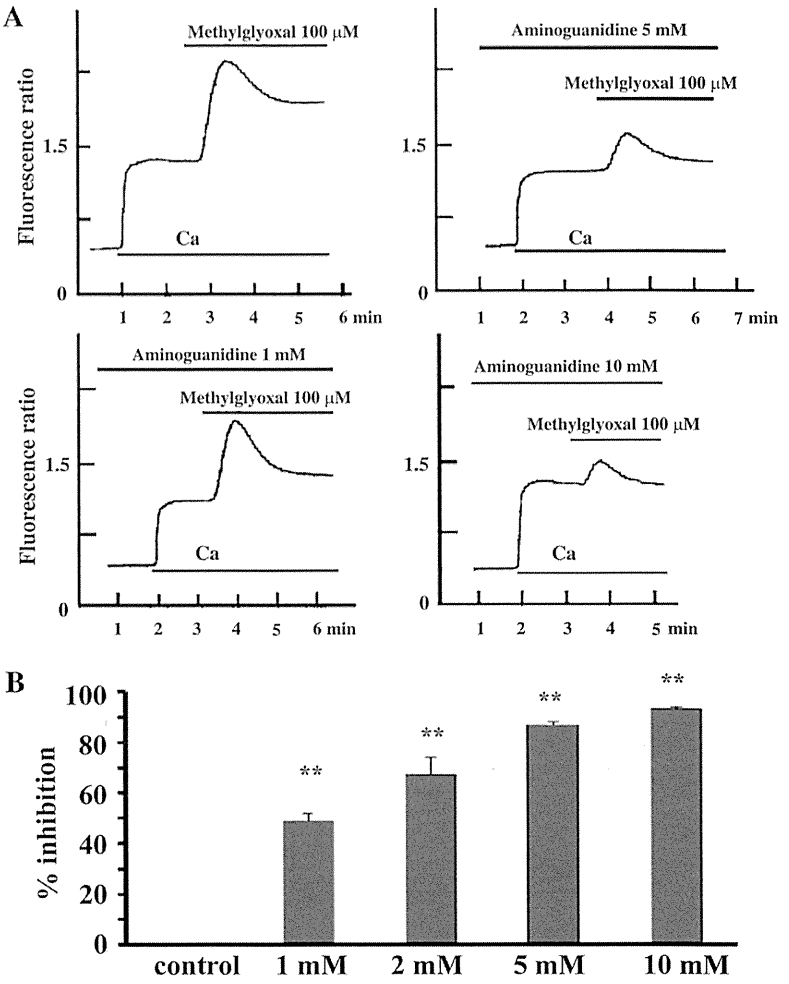

Fig. 6. Effects of aminoguanidine on methylglyoxal-induced $[Ca^{2+}]_i$ entry. *A* and *B*: effects of aminoguanidine on methylglyoxal-induced $[Ca^{2+}]_i$ rise. The cells were pretreated with various concentrations of aminoguanidipne, and then methylglyoxal was added into the bathing solution. The $[Ca^{2+}]_i$ response was compared with the control cells (untreated cells). The typical data are illustrated in *A* control cells and various concentrations of aminoguanidine-treated cells. The data were representative of 4 different experiments. *B*: effects of aminoguanidine on methylglyoxal-induced $[Ca^{2+}]_i$ rise. The increased value in F340/F380 induced by methylglyoxal was obtained in the absence or presence of drugs. The increased value in the absence of drugs is considered as 100%. The percent inhibition of these agents is illustrated in *B*. Each datum represents the mean ± SD of paired 4 different experiments. $^{**}P < 0.01$ vs. control.

progression and differentiation in human cardiac fibroblasts. MG might participate the development of pathophysiological conditions including diabetic cardiomyopathy via activation of TRPA1.

The TRP protein superfamily consists of a diverse group of cation channels in a variety of cells (47) including cardiac fibroblasts, which play an important role on physiological and pathophysiological conditions. In the present study, the expression of TRPV1, TRPV2, and TRPV4 transcripts was detected among TRPVs, and the significant expression of TRPM2, TRPM4, and TRPM7 was observed among TRPMs (data not shown). In addition, the present study provided the first evidence showing that the prominent existence of TRPA1 mRNA was observed in human cardiac fibroblasts, by using the conventional and quantitative real-time RT-PCR analysis. The expression level of mRNA was TRPA1>TRPV2>TRPC1>TRPV1. TRPA1 mRNA appears to be dominantly expressed in human cardiac fibroblasts. And, expression of TRPA1 protein was confirmed by Western blotting and immunocytochemical analyses. From these results, it is very likely that TRPA1 is functionally expressed in human cardiac fibroblasts.

TRPA1 is widely expressed in neuronal and nonneuronal cells (49), (58). The TRPA1 channel is activated by noxious cold (<17°C) and chemical compounds such as mustard oil (38). The present study provided the first evidence showing that the functional expression of TRPA1 was observed in human cardiac fibroblasts. AITC, a selective TRPA1 agonist (38), significantly increased $[Ca^{2+}]i$ in the presence of extracellular Ca^{2+}, while it failed to increase it in the absence of extracellular Ca^{2+}. MG, a dicarbonyl compound, which has been recently shown to activate TRPA1 in rat pancreatic β-cells (13), and PGJ_2, an agent known as another TRPA1 agonist (20), also significantly increased $[Ca^{2+}]i$ as well as AITC. Furthermore, after AITC increased $[Ca^{2+}]i$, the additional application of MG induced a only small increase in $[Ca^{2+}]i$, suggesting that MG and AITC activated the common Ca^{2+}-influx pathways. And, HC030031, a selective TRPA1 antagonist, and ruthenium red, a nonselective TRPA1 blocker, which can block the channel pore, inhibited MG-induced $[Ca^{2+}]i$ increase. The use of siRNA to knock down TRPA1 also markedly reduced the MG-induced Ca^{2+} entry as well as the expression level of TRPA1. Thus these results strongly suggest the involvement of TRPA1 on MG-induced $[Ca^{2+}]i$ increase in human cardiac fibroblasts. However, we have not ruled out the contribution of other ionic channels such as Ca^{2+}-activated K^+

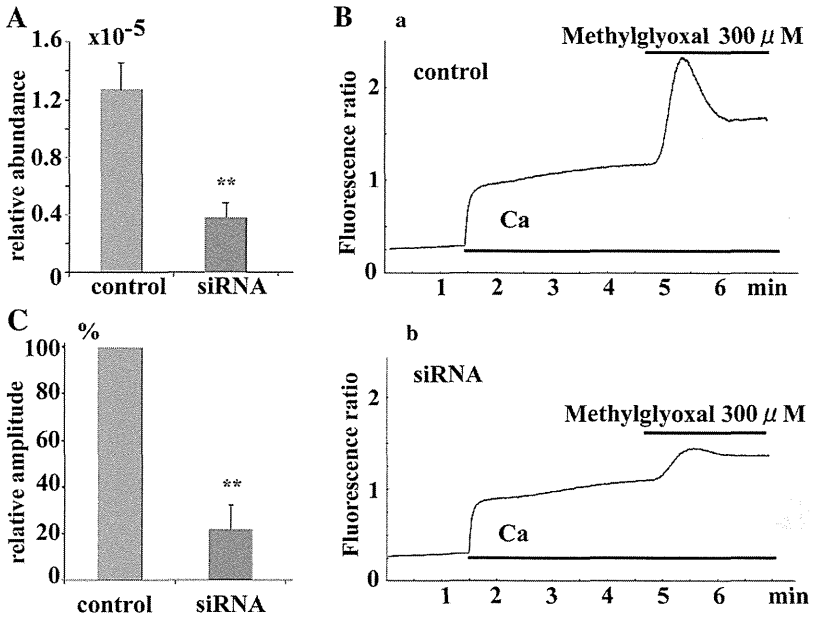

Fig. 7. Effects of treatment with small interfering RNA (siRNA) targeted for TRPA1 on expression level of TRPA1 mRNA and methylglyoxal-induced $[Ca^{2+}]_i$ increase. *A*: effects of treatment with siRNA targeted for TRPA1 on expression level of TRPA1. Human cardiac fibroblasts were treated with siRNA targeted for TRPA1 or control siRNA. Note that siRNA targeted for TRPA1 significantly decreased mRNA level of TRPA1, compared with nonsilence siRNA. $^{**}P < 0.01$ vs. control siRNA. *B* and *C*: effects of siRNA targeted for TRPA1 on methylglyoxal-induced $[Ca^{2+}]_i$ increase. The relative amplitude of methylglyoxal-induced $[Ca^{2+}]_i$ rise are plotted in nonsilence siRNA-treated and siRNA-treated cells. The increased value in nonsilence siRNA-treated cells is considered as 100%. The data were obtained from 3 different cells. $^{**}P < 0.01$ vs. control siRNA.

channels, which are functionally expressed in human cardiac fibroblasts (69), on the MG-induced Ca^{2+} moblilization as described in isolated blood vessel (50).

Long-term diabetes results in the development of diabetic cardiomyopathy. Heart failure due to diastolic ventricular dysfunction is a characteristic of diabetic cardiomyopathy and can occur during the early stages of diabetes (55). Heart cells per se are impaired in diabetic cardiomyoptahy. In addition, cardiac fibrosis is one of the pathological processes of diabetic cardiomyopathy (63) and manifests as enhanced proliferation of cardiac fibroblasts and excessive deposition of ECM, such as collagens and fibronectin. Hyperglycemia, a major pathological manifestation of diabetes, may promote the development of heart failure, primarily by causing excessive accumulation of collagen within the interstices of the myocardium, and then resulting in impaired diastolic and systolic functions (60). Intracellular Ca^{2+} has been reported to be essential for fibroblast functions. Chelating external Ca^{2+} by EGTA prevents substance P-induced proliferation of cultured rat cardiac fibroblasts (43). In human fibroblasts, it has been reported that Ca^{2+} influx is essential for the proliferation, and intracellular Ca^{2+} is required for cell cycle progression from G1/G0 to S phase (64). We have recently shown that human cardiac fibroblasts contain several TRPC-mediated Ca^{2+} influx pathways, and TGF-β_1 enhances the Ca^{2+} influx pathways requiring Ca^{2+} signals for its effect on fibroblast proliferation (35). Several papers have

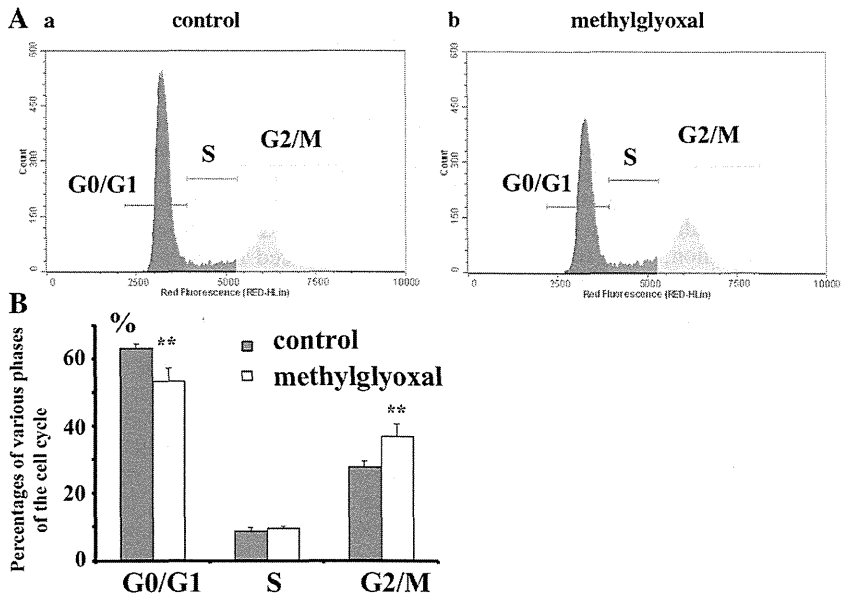

Fig. 8. Effects of methylglyoxal on cell cycle analyzed by flow cytometry. The serum-deprived cells were treated in the absence (*Aa*) or presence (*Aa*) of methylglyoxal for 48 h and analyzed by flow cytometry. Note that methylglyoxal (300 μM) induced G0/G1 to S/G2/M progression. *B*: summary data showing percentage of cells in G0/G1, S, and G2/M under control and the presence of methylglyoxal. The typical data are illustrated in this figure. The typical data obtained from 4 different experiments are illustrated in this figure. Each datum represents the means ± SD of paired 4 different experiments. $^{**}P < 0.01$ vs. control.

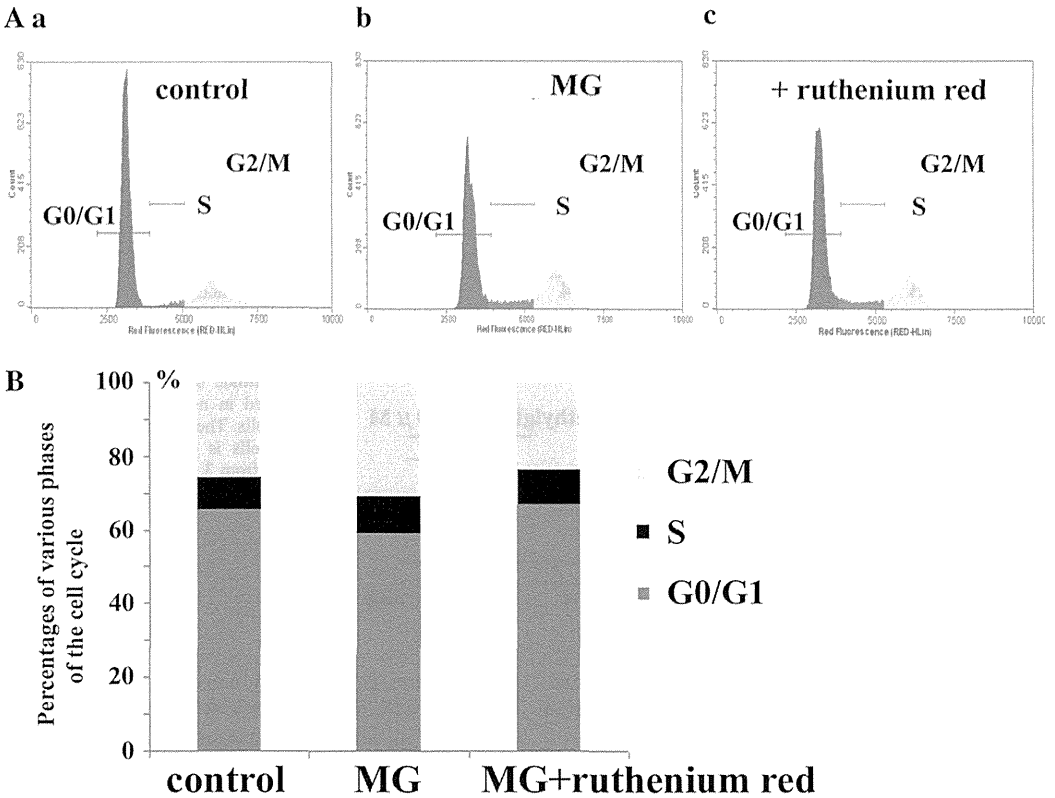

Fig. 9. Effects of ruthenium red on methylglyoxal-induced cell cycle progression analyzed by flow cytometry. The serum-deprived cells were treated in the absence (*Aa*), presence of methylglyoxal (*Ab*), and the additional application of ruthenium red (*Ac*) for 48 h and analyzed by flow cytometry. Note that methylglyoxal (*Ab*; 300 μM) induced cell cycle progression with G0/G1 to S/G2/M progression, compared with control cells (*Aa*). Treatment with ruthenium red (10 μM; *Ac*) showed a smaller proportion of cells entering S and G2/M, and a higher proportion arrested in G0/G1, compared with methylglyoxal by itself (*Ab*). *B*: summary data showing percentage of cells in G0/G1, S, and G2/M under these conditions. Groups: control, methylglyoxal, methylglyoxal plus ruthenium red.

reported that treatment of cardiac fibroblasts with high concentrations of glucose results in increased proliferation and collagen synthesis (5, 66). Dai et al. (21) also reported that high glucose induces the proliferation of cardiac fibroblasts and collagen synthesis via activation of STAT1 and STAT3. Here, we provided the first evidence showing that MG promoted cell cycle progression from G0/G1 to S/G2/M. The MG-induced cell cycle progression was significantly suppressed by treatment with HC030031, a TRPA1 specific blocker, or ruthenium red, a nonspecific TRPA1 blocker, suggesting that TRPA1 is involved in MG-induced cell cycle progression. Similarly, MG-induced cell proliferation has been described in vascular smooth muscle cells and adipocytes (14, 37). In addition, cardiac fibroblasts not only produce the ECM, but also are electrically and mechanically coupled with cardiomyocytes, resulting in affecting the electrical activity (1, 39). They cannot generate action potentials, but their membrane potential is controlled by mechanical stretch or compression of the surrounding myocardium, which in turn affects their interaction with cardiomyocytes. Thus cardiac fibroblasts appear to be dynamic participants in the physiology and pathophysiology of cardiomyocytes. Wang et al. (69) reported the contribution of BK_{Ca}-channel activity in human cardiac fibroblasts to electrical coupling of cardiomyocytes-fibroblasts. Similarly, the activation of TRPA1 induced by MG in cardiac fibroblasts may play a role in affecting electrical activity in cardiomyocytes under the pathophysiological conditions including diabetic cardiomyopathy.

Davis et al. (22) showed an obligate function for TRPC6 in promoting myofibroblast differentiation and wound healing in mice, whereas Harada et al. (32) reported the essential role of TRPC3 on rat cardiac fibroblast proliferation and differentiation. An increase in local Ca^{2+} concentration may trigger protein-protein interactions that activate downstream signaling pathways that regulate fibroblast function such as protein kinase C and ERK1/2 signaling pathway (32). The present study provided the first evidence showing the essential role of TRPA1 on MG-induced fibroblast proliferation and differentiation, but further studies are needed to clarify its downstream signaling pathways as reported in human endothelial cells (2).

After fibroblasts proliferate, they differentiate into ECM-secreting myofibroblasts characterized by altered morphology and increased α-SMA expression. The differentiation of fibroblasts into myofibroblasts is strongly upregulated in failing hearts (12), which is characterized by de novo expression of α-SMA (28). The present study also showed that α-SMA expression in human cardiac fibroblasts was enhanced by MG in a dose-dependent manner. This is compatible with the previous reports in human cardiac fibroblast used collagen gels

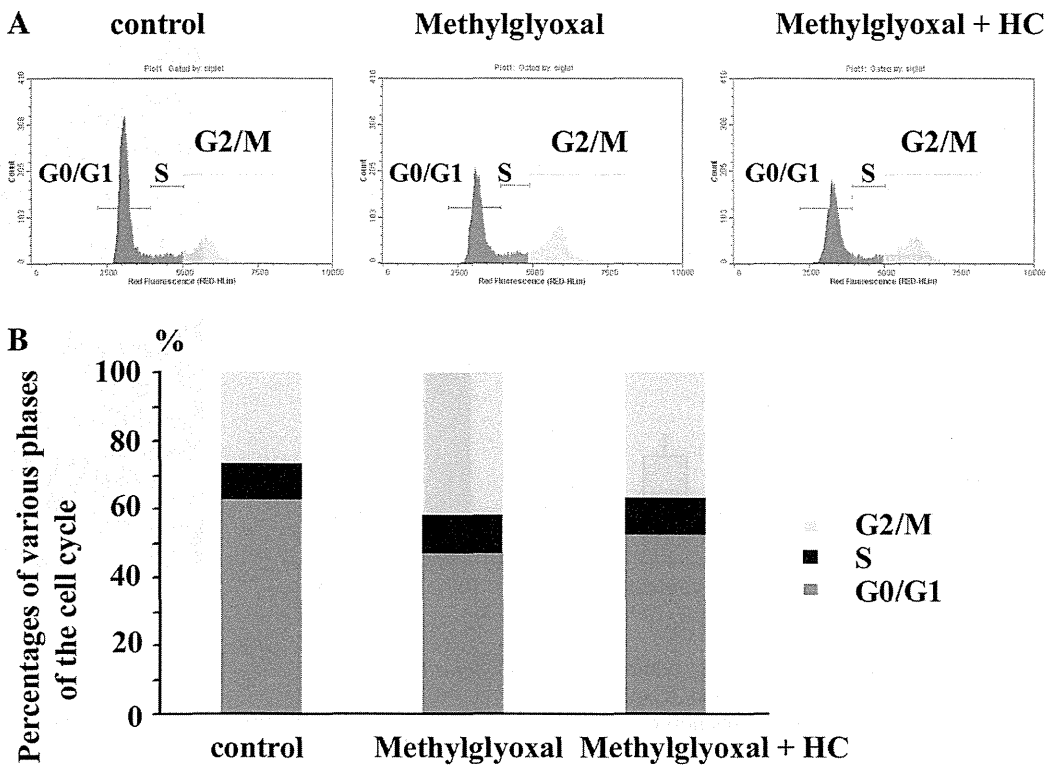

Fig. 10. Effects of HC030031 (HC) on methylglyoxal-induced cell cycle progression analyzed by flow cytometry. The serum-deprived cells were treated in the absence (*Aa*) or presence (*Ab*) of methylglyoxal, and the addition of HC030031 (100 μM) for 48 h, and analyzed by flow cytometry. Note that methylglyoxal (*Ab*; 300 μM) induced cell cycle progression with G0/G1 to S/G2/M progression, compared with control cells (*Aa*). Treatment with HC030031 (100 μM; *Ac*) showed a smaller proportion of cells entering S and G2/M, and a higher proportion arrested in G0/G1, compared with methylglyoxal by itself (*Ab*). *B*: summary data showing percentage of cells in G0/G1, S, and G2/M under these conditions. Groups: control, methylglyoxal, methylglyoxal with HC030031 (100 μM). The typical data are illustrated in this figure.

with 0.01~1 mM MG. Thus MG appears to induce human fibroblasts proliferation and enhance differentiation into myofibroblasts. Based on the results presented in this study, we propose the underlying mechanisms of MG on human cardiac fibroblasts involving the TRPA1 ion channel. Under normal conditions the TRPA1-mediated pathway may act as a low tone system to cause cell proliferation. However, in hyperglycemic conditions, production of MG can directly evoke cell proliferation and differentiation through this pathway, providing a novel signaling mechanism leading to cell proliferation. In addition, MG increased fibronectin production, an ECM (data not shown), suggesting that MG might participate the development of pathophysiological conditions including diabetic cardiomyopathy via activation of TRPA1. Further studies are needed to clarify this possibility.

Plasma levels of MG range from 1.4 to 3.3 μM in healthy humans and from 3.6 to 5.9 μM in patients with diabetes (62, 65). Therefore, MG concentrations (more than 10 μM) used in this study are high. However, it was in the range of those applied by Brouwers et al. (11) and by Cook et al. (19) to rat β-cells. Also, MG concentration of cultured Chinese hamster ovary cells has also been reported to reach up to 310 μM (15). In addition, the intracellular MG level is likely much higher than the plasma MG level in the diabetic condition because diabetic tissues are chronically (months to years) exposed to high MG levels, which may cause dramatic intracellular MG accumulation. In contrast, cultured cells were only transiently (days) exposed to high concentrations of MG, which may limit intracellular MG accumulation (16). Thus the MG concentration range (10–1,000 μM) used in the present study is not only physiologically relevant but also suitable for our in vitro experiments on cultured cells. Further work will be required to examine the longer-term effects of lower doses (~5–10 μM) of MG on the function of cardiac fibroblasts. However, the effects of MG could be antagonized by HC030031, a TRPA1 blocker, RR and he funcsiRNA traged for TRPA1, suggesting that the effects of MG are not mediated by nonspecific toxic effects, but specifically by TRPA1 channel. It has been reported that extracellular applied MG accesses specific intracellular binding sites of TRPA1 and activates it via MG-induced modification of cysteine residues (26). To investigate this possibility whether disulfide bridge formation or reversible noncovalent interactions contribute to the agonist activity of MG, the effect of the reducing agent DTT on methylglyoxal-induced $[Ca^{2+}]_i$ was investigated. DTT is expected to reduce cysteine bridges to free thiols, but also to form hemithioacetals with MG, thereby inhibiting the activation. Treatment with DTT significantly inhibited MG-induced Ca^{2+} entry, suggesting that MG may activate TRPA1 via MG-induced modification of cysteine residues. Further studies are needed to clarify the basic molecular mechanisms underlying the activation of TRPA1 caused by MG.